Food and Bioprocess Technology (2026) 19:100
https://doi.org/10.1007/s11947-025-04182-0

RESEARCH

Region-Specific Spoilage Dynamics in Rainbow Trout Fillets: A Dual Approach Integrating Intelligent Label Response and Sensory Evaluation

Bayram Köstekli[1] · Mehmet Emin Erdem[1] · Can Okan Altan[1] · Bengünur Çorapcı[1] · Rukiye Köklü[1]

Received: 8 August 2025 / Accepted: 15 December 2025 / Published online: 8 January 2026

Abstract

Rainbow trout (*Oncorhynchus mykiss*) fillets are highly perishable due to microbial and biochemical activity; therefore, reliable non-invasive tools are required for real-time freshness monitoring. This study developed and evaluated intelligent labels derived from purple onion peel anthocyanins (POPAS) to monitor the freshness of rainbow trout fillets stored at 4 ± 1 °C. To assess region-specific spoilage dynamics, fillets were divided into head (H), center (C), and tail (T) sections, packaged with intelligent labels, and stored for 15 days. Label responses, including colorimetric indices such as total color difference (ΔE), redness index (RI), whiteness index (WI), and yellowness index (YI) indices, were monitored in relation to pH, in-package CO_2, total volatile basic nitrogen (TVB-N), microbial growth, and sensory quality of both raw and cooked samples. The labels exhibited distinct pH-dependent color transitions: from red (pH 2–3) to pink (pH 4–5), followed by a loss of intensity at pH 6, and finally shifting to green/brownish-green ($pH \geq 7$). Color changes were first visually detectable on day 6 in the T and H groups, corresponding to sensory odor scores falling below the acceptability threshold of 3. By day 12, panelists rejected samples due to odor and chewiness, which coincided with a $\Delta E > 5$ and a label color shift to brownish-green. In-package CO_2 increased from 5.3% on day 1 to approximately 30% on day 15, demonstrating a strong correlation with label color change. Furthermore, ΔE was closely associated with TVB-N and pH variations, highlighting region-specific spoilage dynamics. Intelligent labels developed from POPAS provided a sensitive, non-invasive, and consumer-friendly tool for real-time spoilage detection, showing strong predictive alignment with microbial, chemical, and sensory spoilage limits. Overall, the study highlights the potential of these natural, sustainable colorimetric indicators for seafood safety while introducing a novel approach that reveals region-specific spoilage patterns within a single fillet.

Keywords Intelligent packaging · Sensory quality · Region-specific spoilage · Anthocyanin-based indicator · Purple onion · Freshness monitoring

Introduction

Seafood is highly valued for its nutritional quality; however, it is among the most perishable food categories due to intense microbial activity and enzymatic reactions (Venkatachalam et al., 2025). During storage, the formation of biogenic amines, aldehydes, and sulfides compromises both safety and consumer acceptability. Therefore, monitoring meat quality and safety is essential to minimize potential foodborne risks (Wang et al., 2025a). Beyond food quality and safety, accurately determining the shelf life and the real-time condition of a packaged product is another critical concern. Since shelf life varies depending on handling practices, temperature fluctuations, and environmental factors, it cannot be reliably assessed solely by static expiration

✉ Bayram Köstekli
bkostekli@sinop.edu.tr

Mehmet Emin Erdem
merdem@sinop.edu.tr

Can Okan Altan
okanaltan@sinop.edu.tr

Bengünur Çorapcı
bsoyleyen@sinop.edu.tr

Rukiye Köklü
koklurukiye@gmail.com

[1] Department of Seafood Processing Technology, Faculty of Fisheries, Sinop University, 57000 Sinop, Turkey

dates (Janjarasskul & Suppakul, 2018). These limitations are especially evident in fish fillets, where the head, center, and tail regions may spoil at different rates. This situation underscores the urgent need for rapid, reliable, and consumer-friendly methods to monitor freshness and reduce food safety risks (Boccalon et al., 2022). Consequently, both the food industry and consumers require simple, cost-effective, and practical methods to assess fish freshness after packaging. Concurrently, concerns over plastic waste and the environmental impact of conventional petroleum-based packaging have grown. Collectively, these factors have accelerated interest in innovative, sustainable, and intelligent packaging technologies (Nouraddini et al., 2018).

Driven by technological advancements and rising concerns about food quality and safety, modern packaging has increasingly embraced active and intelligent systems that provide in situ information on product status (Kafashan et al., 2023). Within this scope, various indicators have been developed to monitor meat spoilage, including pH-sensitive indicators (Chen et al., 2025; Dai et al., 2025; Fatehi et al., 2025), biogenic amine indicators (Huang et al., 2025; Wang et al., 2025b; Zamfir et al., 2025), and CO_2 indicators (Far et al., 2025; Kiaitsi et al., 2025). Although pH-responsive colorants are widely employed in these systems, traditionally used synthetic dyes such as methyl red (Basdeki et al., 2025), bromocresol green (Liu et al., 2025), and bromocresol purple (Esmaeili et al., 2025) raise toxicity and food-contact safety concerns (Akbari & Mehregan Nikoo, 2025). As a result, natural pigments—especially anthocyanins from fruits, vegetables, and by-products—have gained traction as safer halochromic alternatives (Almasi et al., 2022; Xue et al., 2025).

Despite this shift, work on purple onion peel anthocyanins (POPAS) remains limited. For example, Devi et al. (2024) successfully developed a biopolymer-based freshness indicator for milk products, demonstrating the feasibility of employing purple onion peel extracts in smart labels; however, this application was restricted to dairy systems, leaving seafood products unexplored. Similarly, Liang et al. (2018) investigated the incorporation of purple onion peel anthocyanins into polymer matrices, providing valuable insights into their rheological properties and film-forming capacity. Notably, while the authors suggested their potential applicability in intelligent packaging as alternatives to synthetic dyes, this study remained at the material characterization level and did not extend to practical validation in real food spoilage models. Huang et al. (2021) also made a significant contribution by developing anthocyanin–polymer complexes and suggesting their potential applicability in monitoring fish spoilage. While this pioneering work laid a foundation, it lacked practical validation on specific fish species, necessitating further research to demonstrate effectiveness in real seafood systems.

Furthermore, few studies have systematically compared the effectiveness of smart labels with sensory analysis, which is crucial for evaluating consumer perception. The work of Kuswandi and Nurfawaidi (2017) stands out as a rare exception, as they combined pH-sensitive indicators with microbial and sensory assessments. This study clearly demonstrated the importance of incorporating sensory evaluation into intelligent packaging research. At the same time, their labels were based on synthetic dyes, and the sensory evaluation was limited to basic parameters, indicating that further refinement and expansion are necessary. Beyond this limited example, the integration of detailed sensory attributes such as appearance, odor, and taste with smart label performance remains largely overlooked, representing a significant gap in the literature.

In this study, intelligent labels derived from POPAS were developed and evaluated for real-time monitoring of rainbow trout fillet freshness. Building upon prior anthocyanin-based indicators, this study examines region-specific spoilage within a single fillet (head, center, and tail sections) and applies a combined validation framework integrating microbiological parameters with detailed sensory evaluation (for both raw and cooked samples). The primary objective was to capture regional spoilage differences through the label responses and to correlate color changes with microbiological and sensory data. Ultimately, this approach clarifies region-specific spoilage patterns as reflected by label color responses and offers a significant contribution to the literature on anthocyanin-based indicators for seafood packaging.

Materials and Methods

Purple onion was purchased from the local market (İstanbul, Turkey). Cellulose filter paper (CFP) (Whatman, No. 1001–047, thickness: 180 µm) was used as the indicator base, serving as a solid support matrix to immobilize and retain the anthocyanin extracts due to its porous and hydrophilic structure. Fresh rainbow trout ($n = 27$, all females—selected to reduce biological variability; weight: 2648.59 ± 24.09 g; length: 54.33 ± 0.34 cm; total weight: 71.5 kg) were harvested by the hypothermia method, in which fish were first crowded in the net pens and then immersed in ice-water slurry at 0–2 °C until loss of reflexes and opercular movements within 3–5 min prior to transportation. The fish were subsequently purchased from a commercial aquaculture facility in Samsun, Türkiye. This procedure is routinely applied at the facility to minimize stress and preserve fillet quality. The facility operates a two-stage aquaculture system, where fish are first raised in freshwater hatcheries under controlled conditions until they reach a weight of 500–600 g. Subsequently, they are transferred to marine net cages in the Black Sea for an additional 6 to

8 months, reaching approximately 20 months of age by the end of this period. The fish were fed a standard commercial pelleted diet supplemented with fishmeal and fish oil. Following harvest, fish were transported to the laboratory in iced styrofoam boxes within 2 h. All chemicals used were of analytical grade and purchased from Merck (Darmstadt, Germany) and used without further purification.

Extraction of Anthocyanins from Purple Onion

Anthocyanins were extracted from purple onion peels according to the method described by Choi et al. (2017), with minor modifications regarding drying temperature and the extraction ratio. Briefly, purple onion peels were manually separated from the inner bulb tissue, washed under tap water for 2 min to remove impurities, and drained in a sieve for 2 h. Subsequently, the peels were dried in a hot-air oven at 37 °C for 6 h until fully dehydrated and ground into a fine powder using a laboratory grinder. For extraction, 100 g of the powder was soaked in 3 L of 40% (v/v) aqueous ethanol to achieve a solid-to-solvent ratio of 1:30 (w/v). The pH of the mixture was adjusted to 2.0 using 1.0 mol L^{-1} hydrochloric acid. The mixture was then stirred continuously in the dark at room temperature (22 ± 2 °C) for 24 h. Following extraction, the solution was filtered to remove insoluble solids, followed by centrifugation at 4000 rpm for 15 min at 4 °C. The resulting supernatant was collected and further filtered through Whatman No. 1001 filter paper. This process was repeated three times, and all supernatants were pooled. The final POPAS solution was stored at 4 °C in the dark for approximately 12 h prior to the preparation of the intelligent labels.

Preparation of Intelligent Labels

Anthocyanins extracted from purple onion peel were immobilized onto cellulose filter papers (CFP) via an absorption method. The CFPs were immersed in anthocyanin solution within petri dishes (90 × 17 mm; 6 pieces per dish, $n = 120$) and kept at 37 °C in the dark for 24 h. During this period, the CFPs were flipped and repositioned every 8 h to ensure uniform distribution, and the anthocyanin solution was replenished as needed (up to a total of 90 mL) to compensate for evaporation. Subsequently, the CFPs were drained for 1 h and air-dried in the dark at room temperature (22 ± 2 °C). The resulting intelligent labels were stored under aseptic conditions at 4 °C, protected from light and moisture until use. To verify manufacturing reproducibility, two independent batches of labels were produced under identical conditions (Lot-1 and Lot-2; 30 labels per lot, total $n = 60$). From each lot, 10 labels were randomly selected. For each selected label, color parameters (L^*, a^*, b^*) were measured in triplicate using a Konica Minolta CR-400 (illuminant D65) and averaged to obtain initial values (L^*_0, a^*_0, b^*_0). The same labels were then exposed to a pH 7.00 buffer for 10–15 s at 22 ± 1 °C and re-measured in triplicate (averaged to L^*_1, a^*_1, b^*_1) to calculate the total color difference (ΔE). Lot-level consistency was deemed acceptable if the standard deviation of ΔE across the 10 labels within a lot was ≤ 0.50. Between-lot reproducibility was confirmed if the absolute difference between the mean ΔE values of the lots ($|\Delta\Delta E|$) was ≤ 1.0 (95% CI).

Formation of Experimental Groups and Integration of Intelligent Labels into Packaging

Fresh rainbow trout were initially scaled, gutted, and washed in cold water. Subsequently, the fish were filleted and skinned, with both fillets from each specimen included in the study. To ensure unbiased allocation, the fillets were randomized and divided into three equal sections based on the anatomical positions of the anal and dorsal fins: head (H), center (C), and tail (T). This anatomical segmentation was designed to reflect region-specific physiology. The head section is relatively better perfused due to its proximity to major vasculature, while the tail section comprises a higher proportion of locomotory muscle with elevated metabolic demand. In contrast, the central region exhibits comparatively lower perfusion. These spatial variations can contribute to region-dependent spoilage patterns, a phenomenon supported by recent hyperspectral analyses and established descriptions of red (highly vascularized) versus white muscle distribution in teleosts (Hardy et al., 2024). All sections were cut into approximately 2 cm^3 cubes under aseptic conditions. To ensure homogeneity, the cubes within each group were thoroughly mixed in separate sterilized containers. Subsequently, 250 g of the mixed samples was transferred into sterilized polypropylene containers (Mono PP, 190 × 144 × 50 mm, weight: 11 ± 5 g, volume: 950 mL, color: transparent, thickness: 440 µm, density: 0.92 g/cm^3, water vapor transmission rate: N/A, oxygen transmission rate: N/A, supplier: Apack, İstanbul, Türkiye). Each container was equipped with a sterile absorbent pad at the bottom (Fig. 1).

Following sample placement, intelligent labels were affixed to the inner side of the PET-PP sealing film (thickness: 12 ± 2 µm, water vapor transmission rate: 8 g/m^2/day, oxygen transmission rate: 25 cc/m^2/day·atm, supplier: Apack, İstanbul, Türkiye) using double-sided adhesive tape. The labels were positioned to face the headspace, ensuring no direct contact with the fish samples. Finally, the packages were hermetically sealed using a Cliopack packaging machine (Clio06, Arı Makina, İstanbul, Türkiye) at 185 °C for 5 s under atmospheric conditions (without gas flushing) and stored at 4 ± 1 °C until further analysis. During sealing, the PET/PP multilayer films were thermally bonded at 185 °C, which could cause outgassing phenomena leading

Fig. 1 Preparation of experimental groups (head, center, tail) and placement of intelligent labels within the packaging

to initial CO_2 levels around 5% even in the absence of biological activity. To verify this, empty packages (without fish samples) prepared under the identical conditions were used as controls to monitor CO_2 variations and label color stability over the 15-day storage period. The CO_2 concentration in these control packages remained stable ($5 \pm 1\%$) throughout storage, confirming that the initial CO_2 levels were attributable to outgassing from the PET/PP film rather than microbial respiration.

Analyses

A total of 40 packages were prepared for each experimental group, divided into two independent subsets of 20 packages to serve as replicates. On each designated sampling day, two packages were randomly selected from each group for analysis. Proximate composition analyses were conducted on raw fish samples at the beginning of the study (day 0) and subsequently at three-day intervals throughout the storage period ($n = 6$). The ammonia response of the intelligent labels was assessed exclusively at the beginning of the study ($n = 6$). Daily monitoring over the 15-day storage period included colorimetric analysis ($n = 8$), headspace gas composition ($n = 2$), total volatile basic nitrogen (TVB-N) ($n = 10$), and pH measurements ($n = 6$). Regarding gas composition, the destructive nature of the analysis (film perforation by the sampling needle) limited measurements to one per package to prevent leakage; therefore, gas composition results represent $n = 2$ per group per sampling day. Furthermore, microbiological analyses ($n = 4$) and sensory evaluations ($n = 20$) were conducted daily throughout the storage period.

Colorimetric Analysis

The colorimetric response of the intelligent labels containing POPAS was evaluated according to the method described

by Ghanbarzadeh et al. (2010), with minor modifications. Label samples (2 cm^2) were immersed for 5 min in 10 mL of buffer solutions ranging from pH 2 to 10. Specifically, 0.1 M HCl was used for pH 2–6, distilled water for pH 7, and 0.1 M NaOH for pH 8–10. Visual documentation of the color transitions was captured using a smartphone camera (iPhone 14; Apple Inc., USA). Subsequently, quantitative color measurements were performed using a Konica Minolta CR-400 chromameter (light projection tube model: A33a, Tokyo, Japan). Following calibration, the CIE color coordinates—L* (lightness), a* (red–green), and b* (yellow–blue)—were recorded. Based on these values, the total color difference (ΔE), whitening index (WI), redness index (RI), and yellowing index (YI) were calculated according to Eqs. (1–4).

$$\Delta E = \sqrt{\left(L_0^* - L^*\right)^2 + \left(a_0^* - a^*\right)^2 + \left(b_0^* - b^*\right)^2} \quad (1)$$

$$WI = \sqrt{(100 - L)^2 + a^2 + b^2} \quad (2)$$

$$\mathrm{RI} = a^*/b^* \quad (3)$$

$$\mathrm{YI} = (142.86 \times b^*)/L^* \quad (4)$$

In which L_0, a_0, and b_0 are the color parameters of each indicator in its natural state, and L^*, a^*, and b^* are the color indexes of each label at the exposed pH levels after 5 min.

In addition to the standard pH buffer assays, the colorimetric behavior of the intelligent labels was monitored under real packaging conditions throughout the storage period. On each sampling day, following in-package CO_2 measurement and microbiological sampling, color measurements were performed directly on the labels affixed to the inner surface of the PET-PP films. To ensure representative data, readings were taken at four distinct locations on each label surface using the previously described chromameter. This procedure allowed for the accurate assessment of the in situ halochromic response triggered by spoilage-associated volatiles accumulating within the package headspace.

Total Anthocyanin Content

The total anthocyanin content of the purple onion peel extract was determined using the pH differential method described by Lako et al. (2007), with minor modifications. Briefly, 0.4 mL of the extract was mixed separately with 3.6 mL of potassium chloride buffer (0.025 M, pH = 1.0) and sodium acetate buffer (0.4 M, pH = 4.5). After 15 min of equilibration at room temperature, the absorbance of each mixture was measured at 510 and 700 nm using a UV–Vis spectrophotometer (Shimadzu, UV-2600). Total anthocyanin content was calculated as mg cyanidin-3-glucoside equivalents/100 mL of extract using Eqs. (5) and (6).

$$A = (A510 - A700)_{pH:1} - (A510 - A700)_{pH:4,5} \quad (5)$$

$$\textit{Total anthocyanin content}\ (mg/100mL) = \frac{A \times MW \times 100}{MA} \quad (6)$$

where A is the absorbance, MW is the molecular weight (449.2 g/mol), and MA is the molar absorptivity of cyanidin-3-glucoside (26,900).

Intelligent Labels Response to Ammonia

The sensitivity of the intelligent labels to volatile ammonia was assessed according to the protocol described by Zhang et al. (2019). Briefly, 80 mL of 0.8 M ammonia solution was transferred into an Erlenmeyer flask, and each label was suspended 1 cm above the liquid surface. The halochromic response was measured immediately after exposure using a Konica Minolta CR-400 chromameter (light projection tube model: A33a, Tokyo, Japan). The sensitivity (S_{RGB}) of the intelligent labels to ammonia was calculated according to Eq. (7), where R_a, G_a, and B_a represent the initial RGB values (before exposure), and R_b, G_b, and B_b denote the RGB values recorded after exposure.

$$\Delta R = \left|R_a - R_b\right|$$

$$\Delta G = \left|G_a - G_b\right|$$

$$\Delta B = \left|B_a - B_b\right|$$

$$S_{\mathrm{RGB}} = \left(\frac{\Delta R + \Delta G + \Delta B}{R_a + G_a + B_a}\right) \times 100 \quad (7)$$

In-Pack CO_2 Measurements

The CO_2 concentration in the package headspace was quantified using a portable gas analyzer (WittOxyBaby M/CO_2; Witten, Germany). For analysis, the device's needle probe was carefully inserted through the sealing film, and measurements were recorded automatically upon stabilization, as indicated by the device's audible signal. Due to the destructive nature of this method—specifically, the compromise of package integrity via needle puncture—measurements were restricted to two independent packages per group for each sampling interval ($n = 2$).

Measurement of pH and Total Volatile Basic Nitrogen

The pH values of the fish samples were measured using a digital pH meter (WTW, Model Profiline 3110), equipped with a glass electrode. Measurements were performed directly on the homogenized samples subsequent to microbiological analysis. Total volatile basic nitrogen (TVB-N) content was determined according to the method described by Ludorf and Meyer (1973). Briefly, 2 g of homogenized sample was transferred into distillation tubes, followed by the addition of magnesium oxide (MgO; 0.5–1 g) and 100 mL of distilled water. Distillation was conducted using a nitrogen/protein macro-distillation unit (Şimşek, 1106-DEST, Ankara, Türkiye). The distillate was collected in a receiver flask containing a mixture of 5 mL of 3% boric acid (H_3BO_3), 100 mL of distilled water, and 4 drops of Tashiro's indicator. Distillation proceeded until 100 mL of distillate was obtained. The collected solution was then titrated with 0.1 N HCl. The volume of HCl consumed to reach the endpoint (indicated by color change) was recorded, and the TVB-N concentration was calculated using the following equation:

$$TVB-N(mg/100g\ sample) = \frac{titrated\ HCl(mL) \times normality\ of\ HCl(0.1) \times milli\ quivalent\ of\ nitrogen\ (N=0.014)}{Weight\ of\ sample} \times 100 \quad (8)$$

Microbiological Analyses Microbial counts were determined according to standard protocols. Total mesophilic aerobic bacteria (TMAB) and total psychrophilic aerobic bacteria (TPAB) counts were assessed following AOAC (2000) methods (ref. no. 966.23b and 966.23c). Counts for *Pseudomonas* spp., total coliforms (TC), lactic acid bacteria (LAB), and total yeast and mold (TYM) were determined according to the methods described by Brown and Lowbury (1965), Halkman (2005), and Kostaki et al. (2009). Confirmatory biochemical tests (catalase, oxidase, coagulase, and Gram staining) were performed as described by Halkman (2005).

TMAB and TPAB were enumerated on Plate Count Agar (PCA) using the spread-plate method (0.1 mL dilutions). TMAB plates were incubated at 37 °C for 48 h, while TPAB plates were incubated at 7 °C for 10 days. *Pseudomonas* spp. were isolated on *Pseudomonas* selective agar base (Cetrimide Agar supplemented with 10 mL glycerol), incubated at 35 °C for 48 h; oxidase-positive colonies were recorded as *Pseudomonas* spp. Total coliforms were enumerated on Violet Red Bile Agar (VRBA) using the overlay method and incubated at 35–37 °C for 18–24 h; typical colonies surrounded by a red precipitate zone were counted as coliforms. Lactic acid bacteria (LAB) were cultured on de Man Rogosa Sharpe (MRS) agar at 37 °C for 72 h; cream-colored, Gram-positive, and catalase-negative colonies were identified as LAB. Yeasts and molds were enumerated on Potato Dextrose Agar (PDA) after incubation at 28 °C for 72 h. All microbial counts were transformed into logarithms of colony-forming units per gram (log CFU/g).

Sensory Analysis

Sensory analysis was conducted in two consecutive stages (on raw and cooked samples) on each sampling day to evaluate the freshness and quality of fish samples from the T, C, and H groups. The sensory panel consisted of 10 trained assessors recruited from the Department of Fish Processing Technology, comprising both academic staff and postgraduate students. Panelists were selected based on their prior experience (> 10 sensory trials), sufficient knowledge of fish freshness criteria, regular fish consumption habits (≥ 2 times per week), and absence of fish-related allergies. Gender balance was maintained, though no specific age stratification was applied. Given the panelists' prior experience, specific training was not deemed necessary, but a briefing on the study objectives was provided. Evaluations were conducted individually and independently under room temperature conditions, without contact or communication between panelists.

In the first stage, following in-pack CO_2 measurement, microbiological sampling, and label color measurement, random portions (50 g) of raw fish from each group (T, C, H) were presented on white porcelain plates. Panelists assessed appearance, odor, color, and texture using a modified 10-point hedonic scale (York & Sereda, 1994). The scale was defined as follows: ≥ 9 (highly liked), 7–9 (liked), 4–6 (moderately liked), and 1–3 (unacceptable/below consumption threshold). To verify panel reliability, blind duplicate samples were also provided to each assessor. Panelists were unaware that these portions originated from the same sample, and the duplicate scores showed high consistency and were averaged with the other ratings.

In the second stage, immediately following the raw evaluation, the same portions were cooked in sealed glass jars in a boiling water bath for 20 min and cooled to 50 °C at room conditions. The sealed jar method was employed to minimize the loss of volatile compounds, thereby preserving the intrinsic aroma and flavor profiles for accurate assessment. No additives (salt, spices, or oil) were used to avoid

masking the natural sensory properties. Cooked samples were rated for oil color, odor, flesh texture, chewing characteristics, and flavor on a 3-point scale: ≥ 2.7 (very good), 2.0–2.7 (good), 1.0–2.0 (fair), and 0–1.0 (spoiled). Sensory analysis of cooked samples was discontinued on days when raw samples were rated as spoiled, as they were deemed unfit for human consumption. All scores were averaged across the 10 panelists, without excluding outliers. Because repeated measures on the same sample over time were infeasible, sensory reliability was assessed as inter-rater agreement: parallel scores from different panelists were analyzed using ICC(2,k) (two-way random-effects, absolute agreement) with 95% confidence and Kendall's coefficient of concordance (W) for ordinal attributes. All participants provided written informed consent prior to participation.

Proximate Composition Analysis

Moisture, crude protein, and ash contents were determined using standard analytical procedures described by AOAC (1995), whereas crude fat content was quantified according to the AOAC (2005) method.

Statistical Analysis Results are expressed as means ± standard deviation (SD). Prior to statistical comparison, the assumptions of normality and homogeneity of variance were verified using the Shapiro–Wilk and Levene's tests, respectively. Differences among experimental group means were assessed via one-way analysis of variance (ANOVA), followed by Tukey's post hoc test for multiple comparisons, with statistical significance accepted at $p < 0.05$. These analyses were conducted using Minitab software (Version 21.1; Minitab Inc., State College, PA, USA) (Sümbüloğlu & Sümbüloğlu, 2007). Additionally, Pearson's correlation coefficient (r) was calculated to evaluate the relationships between the colorimetric responses of the intelligent labels and the physicochemical, microbiological, and sensory spoilage indicators. Correlation analyses were performed using IBM SPSS Statistics (Version 24.0; IBM Corp., Armonk, NY, USA), with significance levels established at $p < 0.05$ and $p < 0.01$.

Results and Discussions

Color Response of Intelligent Labels and POPAS Solution

The total anthocyanin content of the POPAS solution was determined to be 11.74 ± 0.03 mg/100 mL.

The color variations of the POPAS solution across a broad pH range (pH 2–14) are presented in Fig. 2a. Preliminary evaluations revealed distinct color transitions: under highly acidic conditions (pH 2–3), the solution displayed a dark red hue, which progressively shifted to a pinkish tone as the pH increased to 5. At pH 6, the solution transitioned to a light green hue. In alkaline conditions, the color shift intensified, resulting in a brownish-green appearance up to pH 11, while pH values between 12 and 14 yielded a yellowish-green color. These variations are governed by the structural modifications of anthocyanins in different pH environments: transforming from the flavylium cation (pH < 3) to the quinonoidal anhydrobase (pH 4–7), the chalcone (pH 8–9), the carbinol base (pH 10–11), and finally the yellow chalcone (pH 12), all of which contribute to the broad color spectrum observed (Koshy et al., 2021). Although the POPAS solution exhibited two primary color phases—red in the acidic range and green in the alkaline range—intermediate hues such as pink, green, brownish-green, and yellowish-green were distinctly discernible to the naked eye. Notably, the prominent color transition observed in the pH 6–7 interval closely corresponds to the pH range associated with fish spoilage. This alignment highlights the potential applicability of purple onion peel-derived anthocyanins as natural indicators in pH-responsive intelligent label systems for the real-time monitoring of fish freshness. The observed color changes in POPAS are consistent with previous reports (Huang et al., 2021; Roy & Rhim, 2021).

The intelligent labels also demonstrated distinct and visually perceptible color transitions across the tested pH range (pH 2–10). When exposed to strongly acidic buffer solutions (pH 2–3), the labels exhibited a red coloration, which gradually shifted to pinkish tones between pH 3 and 4. At pH 5 and 6, the color intensity noticeably faded, followed by the emergence of green hues beyond pH 7–8 (Fig. 2b). These colorimetric changes were attributed to the structural transformations of the extracted anthocyanins from purple onion peel, particularly the transition from the flavylium cation to the quinonoidal base form, which resulted in a reduction of red intensity. At pH values above 8.0, the degradation of anthocyanins in the alkaline environment led to the formation of a dark green color. This visual behavior was supported by instrumental measurements, where a gradual decrease in the whiteness index (WI) was observed from pH 2 to 10, indicating a shift away from ideal whiteness as the hue transitioned from red to green. Furthermore, a sharp decline in the redness index (RI) starting at pH 5 confirmed the loss of red dominance under neutral to basic conditions (Fig. 2c). According to Tirtashi et al. (2019), color differences become visually perceptible when the total color difference (ΔE) exceeds 5, a criterion that further supports the visual detectability of the pH-induced transitions observed in this study.

As illustrated in Fig. 2a and b, the color transition patterns of the intelligent labels showed slight deviations from those observed in the POPAS. Notably, both hue and

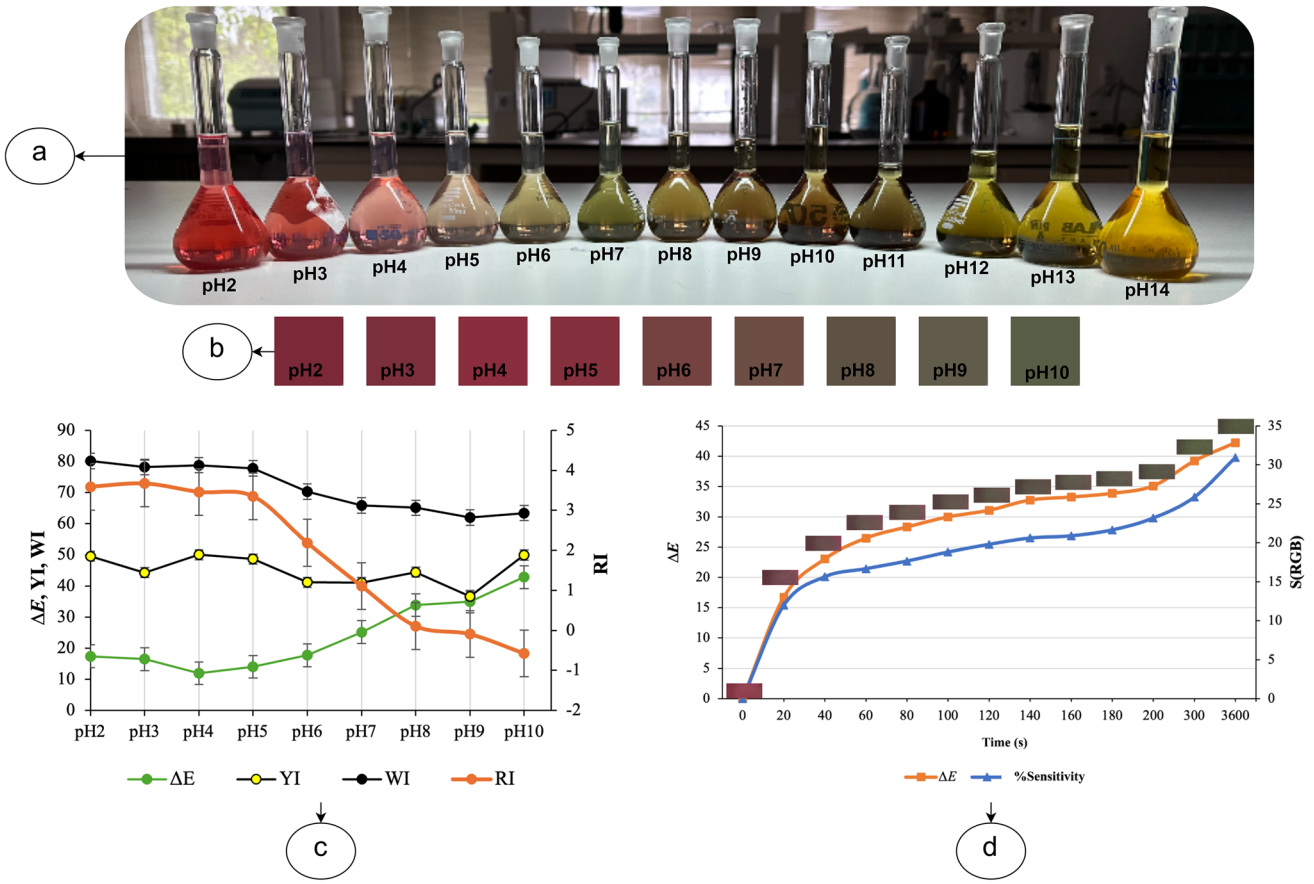

Fig. 2 Colorimetric response of the POPAS solution and intelligent labels under varying pH conditions and their sensitivity to ammonia vapor. **a** Visual color transitions of the POPAS solution. **b** Visual appearance of the intelligent labels (pH 2–10). **c** Δ*E*, YI, WI, and RI values of labels across the pH range. **d** Sensitivity of the labels to ammonia exposure ($n = 6$)

intensity of the color response varied between the liquid and solid phases. These differences may be attributed to hydrogen bonding interactions between the anthocyanin molecules and the hydroxyl groups within the cellulose-based filter paper matrix. Such interactions can alter anthocyanin conformation and, consequently, modulate their halochromic behavior (Forghani et al., 2023). The pH-responsive behavior observed in this study aligns well with the color transitions reported by Choi et al. (2017), although minor differences in hue and transition intervals may be due to variations in the source and structural characteristics of the anthocyanins used.

Sensitivity of Intelligent Labels to Ammonia

Rapid and distinct color change is a key characteristic of pH-responsive freshness indicators. The high ammonia sensitivity of anthocyanin-based intelligent labels is attributed to structural changes driven by hydroxyl ions and the presence of polyphenolic groups (Ezati & Rhim, 2020). Therefore, ammonia sensitivity analysis was performed as a screening test to evaluate the color response of the indicators in the presence of volatile compounds, simulating conditions of protein-rich food spoilage. Upon exposure to ammonia vapor, the anthocyanin-loaded intelligent labels exhibited a rapid color change from red to burgundy and subsequently to green within 1 h (Fig. 2d). The measured sensitivity increased significantly from 11.98 to 30.96% over the 1-h period, indicating a strong responsiveness to ammonia. Similarly, Taherkhani et al. (2020) reported a 67% sensitivity after just 4 min of exposure using a bacterial cellulose-based indicator containing anthocyanins. In another study, Zhang et al. (2019) observed a 30% sensitivity after 16 min of ammonia exposure in a rose anthocyanin-based indicator composed of starch, chitosan, and polyvinyl alcohol. Since ammonia is a major volatile compound associated with spoilage in protein-rich foods, the rapid color response of the labels confirms their suitability for detecting early spoilage in fish packaging.

pH, TVB-N and In-Pack CO_2 Measurement Results

During refrigerated storage, the pH, total volatile basic nitrogen (TVB-N), and in-package CO_2 levels of rainbow

trout fillets increased progressively, reflecting the progression of microbial and biochemical spoilage (Table 1). The pH value is a critical indicator of fish freshness, as it reflects the biochemical changes occurring during storage. As spoilage progresses, the microbial degradation of proteins leads to the formation of volatile basic compounds such as trimethylamine, dimethylamine, and ammonia. The gradual accumulation of these compounds contributes to pH elevation over time (Huang et al., 2021). As presented in Table 1, the initial pH values of 6.74 and 6.56 were recorded for the T and H groups, respectively. From the 10th day onwards, the pH in these groups exceeded 6.8, reaching values above 7.0 by day 12, which indicated the onset of spoilage. This increase coincided with noticeable color changes in the intelligent labels, particularly the transition from pink to green hues. This rise in pH is consistent with microbial proteolysis, which generates alkaline volatiles (ammonia and other amines; TVB-N) that elevate muscle pH and are subsequently captured by the pH-responsive indicators (Khan et al., 2024). Similarly, Aghaei et al. (2020) reported a gradual increase in pH from 6.46 to 6.90 in rainbow trout over 12 days, attributing this to protein hydrolysis and the formation of alkaline metabolites. In their study, color changes were delayed until day 6, manifesting as a slight shift to a purplish hue.

In addition to pH, Yoshida et al. (2014) reported that various factors can influence food shelf life, noting that chemical reactions and microbial growth affecting flavor, stability, and longevity also contribute to pH changes in food. TVB-N serves as a critical index of spoilage, reflecting the accumulation of volatile basic compounds—including ammonia, methylamine, dimethylamine, and trimethylamine—generated through microbial activity during cold storage or the enzymatic degradation of proteins (Hsiao & Chang, 2017). Therefore, TVB-N analysis was conducted in this study to further evaluate the extent of protein degradation and spoilage. TVB-N values increased from initial levels < 16 mg/100 g to > 35 mg/100 g by day 13 in the T and H groups, thereby surpassing the commonly accepted spoilage threshold. Distinct color transitions in the intelligent labels became discernible on days 10–11. This coincided with the sharp acceleration in TVB-N and pH values, suggesting that the label response effectively mirrored the onset of chemical spoilage. Furthermore, these transitions corresponded with sensory evaluations, which revealed strong off-odors in the T and H groups by day 10. These findings parallel those of

Table 1 Temporal variation of TVB-N, pH, in-package CO_2 concentrations, and colorimetric responses of intelligent labels in distinct fillet portions

Days	TVB-N (mg/100g)			pH			In-pack CO_2 content (%)*			Response Color of Labels		
	T	C	H	T	C	H	T	C	H	T	C	H
0	15.83 ± 0.35^{Ajk}	15.58 ± 0.24^{Aij}	15.37 ± 0.61^{Aij}	6.74 ± 0.05^{Acde}	6.69 ± 0.09^{Afg}	6.56 ± 0.04^{Aij}	5.30 ± 0.00^{Ak}	5.30 ± 0.00^{Ah}	5.40 ± 0.00^{Ak}			
1	14.67 ± 0.31^{Ak}	14.96 ± 0.36^{Aj}	13.16 ± 0.39^{Bj}	6.64 ± 0.01^{Be}	6.70 ± 0.02^{Afg}	6.63 ± 0.00^{Bhi}	8.40 ± 0.00^{Aj}	8.40 ± 0.05^{Ag}	8.60 ± 0.05^{Aj}			
2	15.15 ± 0.29^{Bk}	16.99 ± 0.14^{Ahi}	15.91 ± 0.53^{ABi}	6.32 ± 0.03^{Af}	6.23 ± 0.01^{Ai}	6.32 ± 0.01^{Ak}	9.60 ± 0.00^{Aij}	8.90 ± 0.35^{Afg}	9.30 ± 0.10^{Aj}			
3	18.04 ± 0.23^{Bi}	15.34 ± 0.11^{Cj}	20.38 ± 0.15^{Ah}	6.39 ± 0.01^{Af}	6.18 ± 0.01^{Cj}	6.23 ± 0.01^{Bl}	10.30 ± 0.15^{Aij}	10.00 ± 0.10^{Afg}	10.70 ± 0.10^{Aij}			
4	20.93 ± 0.43^{Ai}	17.63 ± 0.22^{Bh}	20.98 ± 0.40^{Ah}	6.40 ± 0.02^{Bf}	6.36 ± 0.02^{Bhi}	6.51 ± 0.01^{Aj}	10.70 ± 0.05^{Aij}	9.70 ± 0.25^{Bfg}	9.80 ± 0.10^{ABj}			
5	21.95 ± 0.37^{Ag}	19.43 ± 0.11^{Bg}	21.51 ± 0.29^{Agh}	6.71 ± 0.02^{Ade}	6.43 ± 0.01^{Bh}	6.71 ± 0.08^{Afg}	11.20 ± 0.20^{Ahi}	10.40 ± 0.10^{Af}	10.70 ± 0.15^{Aij}			
6	23.63 ± 0.21^{Ah}	22.06 ± 0.09^{Bf}	22.57 ± 0.24^{Bg}	6.70 ± 0.01^{Ade}	6.68 ± 0.01^{Ag}	6.57 ± 0.02^{Bij}	11.70 ± 0.10^{Ahi}	10.10 ± 0.00^{Bfg}	12.60 ± 0.25^{Ahi}			
7	25.55 ± 0.43^{Ag}	22.78 ± 0.23^{Bf}	26.60 ± 0.32^{Af}	6.65 ± 0.02^{Be}	6.72 ± 0.00^{Afg}	6.66 ± 0.00^{Bgh}	13.60 ± 0.40^{Ah}	10.20 ± 0.10^{Bf}	13.60 ± 0.43^{Ah}			
8	29.27 ± 0.46^{Aef}	25.61 ± 0.29^{Bde}	25.92 ± 0.10^{Bf}	6.78 ± 0.01^{Bcd}	6.84 ± 0.00^{Ae}	6.76 ± 0.01^{Bef}	16.50 ± 0.15^{Bg}	10.50 ± 0.15^{Cf}	20.80 ± 0.05^{Ag}			
9	28.95 ± 0.27^{Aef}	25.52 ± 0.28^{Bc}	28.21 ± 0.26^{Ae}	6.84 ± 0.00^{Ac}	6.85 ± 0.00^{Ae}	6.82 ± 0.00^{Bc}	22.80 ± 0.95^{Af}	10.70 ± 0.15^{Bf}	23.00 ± 0.30^{Afg}			
10	28.34 ± 0.33^{Af}	25.75 ± 0.55^{Bde}	29.53 ± 0.40^{Ae}	6.81 ± 0.01^{Acd}	6.76 ± 0.01^{Bf}	6.83 ± 0.01^{Ae}	21.80 ± 0.10^{Bf}	14.40 ± 0.50^{Ce}	24.80 ± 0.10^{Aef}			
11	30.36 ± 0.35^{Ade}	25.80 ± 0.17^{Bde}	31.18 ± 0.21^{Ad}	7.04 ± 0.06^{Ab}	6.97 ± 0.01^{Acd}	7.06 ± 0.00^{Ad}	26.70 ± 0.90^{Ae}	15.80 ± 0.30^{Be}	23.40 ± 1.00^{Af}			
12	31.88 ± 0.50^{Ad}	26.89 ± 0.35^{Bd}	31.82 ± 0.35^{Ad}	7.11 ± 0.01^{Ab}	6.93 ± 0.00^{Bd}	7.15 ± 0.03^{Ac}	24.30 ± 0.20^{Aef}	15.90 ± 0.05^{Be}	24.80 ± 0.35^{Aef}			
13	35.06 ± 0.10^{Ac}	30.52 ± 0.17^{Bc}	35.37 ± 0.21^{Ac}	7.30 ± 0.04^{Ba}	7.02 ± 0.01^{Cc}	7.40 ± 0.01^{Ab}	26.30 ± 0.20^{Ae}	20.80 ± 0.60^{Bd}	26.00 ± 0.90^{Ae}			
14	38.27 ± 0.13^{Ab}	33.07 ± 0.21^{Bb}	37.53 ± 0.41^{Ab}	7.35 ± 0.02^{Ba}	7.18 ± 0.01^{Cb}	7.44 ± 0.02^{Aab}	26.10 ± 0.30^{Be}	21.40 ± 0.34^{Cd}	29.60 ± 0.05^{Ad}			
15	43.75 ± 0.26^{Aa}	36.56 ± 0.21^{Ba}	44.41 ± 0.20^{Aa}	7.41 ± 0.02^{Ba}	7.30 ± 0.01^{Ca}	7.49 ± 0.02^{Aa}	32.10 ± 0.55^{Ad}	24.50 ± 0.45^{Bc}	30.10 ± 0.35^{Acd}			

Mean ± SD. CO_2 ($n = 2$), TVB-N ($n = 10$), pH ($n = 6$). A, B, C (→): Different uppercase superscript letters within the different column indicate significant differences between groups ($p < 0.05$). a, b, c … f (↓): Different lowercase superscript letters within the same column indicate significant differences between days ($p < 0.05$). *CO_2 values in control (without-fish) packages remained constant at approximately 5 ± 0.1% throughout the 15-day storage, confirming no biological CO_2 generation

Wells et al. (2019), who demonstrated that TVB-N accumulation within the package headspace triggers colorimetric changes in anthocyanin-based labels. In the present study, two distinct color transitions were observed over the 15-day storage period; these were significantly correlated with the TVB-N content of the fillets and remained consistent with the halochromic patterns previously established in the buffer solution tests.

Microbial activity is the primary driver of spoilage, leading to the production of volatile compounds such as carbon dioxide, ammonia, dimethylamine, and trimethylamine, which accumulate in the package headspace. Therefore, monitoring the headspace composition provides critical data regarding product freshness (Hassanpour et al., 2022). To track spoilage progression, daily headspace CO_2 measurements were conducted throughout the storage period. In control packages (day 0), CO_2 levels were approximately 5% and remained stable throughout storage, consistent with reports for air-packed seafood (Kocatepe et al., 2016). In contrast, the experimental packages exhibited a marked rise in CO_2 levels. Specifically, the T and H groups showed a significant increase starting from day 7, reaching 21.8% and 24.8% by day 10, and peaking at 30.1–32.1% on day 15. This trend aligns with the existing literature, where oxygen depletion and CO_2 accumulation occur due to microbial respiration and gas exchange dynamics within the food–film system (Martin et al., 2023).

Conversely, the C group exhibited a delayed increase, with CO_2 levels rising only after day 9 and reaching approximately 24.5% by day 15, likely reflecting slower microbial proliferation in this region. While the general spoilage trend was consistent across all anatomical regions, the kinetics were notably more rapid in the tail samples. In the C group, spoilage indicators followed a similar trajectory: pH increased from 6.69 (day 0) to 7.30 (day 15), while TVB-N rose from 15.58 to 36.56 mg/100 g. Similarly, headspace CO_2 increased from 5.3 to 24.5%. Although color transitions in the intelligent labels were slightly delayed compared to the T and H groups, distinct greenish hues were evident by day 11. These results indicate that the intelligent label was effective in detecting spoilage even in minimally processed raw samples.

The total color difference (ΔE) of the intelligent labels exhibited strong positive correlations with established spoilage indicators across all sample groups. In the tail, center, and head regions (corresponding to the T, C, and H groups), ΔE values increased in parallel with rising TVB-N, pH, and CO_2 levels. The strongest overall correlation was observed between ΔE and CO_2 in the C group ($r = 0.977$), followed by the T group ($r = 0.951$) and the H group ($r = 0.941$). The central region, characterized by higher protein content and a more uniform tissue structure, may have supported more consistent microbial activity and CO_2 accumulation, resulting in the strongest correlation with label color shift. Similarly, the highest correlation between ΔE and TVB-N was found in the tail group ($r = 0.930$), which also showed the greatest reduction in protein content during storage—an indication of intense proteolytic activity, as supported by the proximate composition data (Table 2). The strongest correlation with pH occurred in the head group ($r = 0.911$), likely due to its softer tissue and higher fat content, which may have promoted faster pH shifts. These findings confirm that label color change closely reflects spoilage progression, support the indicator's effectiveness in tracking both chemical and microbial deterioration across different anatomical regions of fish fillet.

Table 2 Changes in proximate composition of groups (g/100 g)

	Groups	Days				
		0	6	9	12	15
Moisture	**T**	67.06 ± 0.15^{Aa}	65.85 ± 0.20^{Aa}	65.7 ± 0.21^{Aa}	66.65 ± 0.21^{Aa}	66.23 ± 1.06^{Aa}
	C	63.73 ± 0.56^{Cc}	65.92 ± 0.20^{Aa}	66.32 ± 0.17^{Aa}	65.18 ± 0.39^{Bac}	64.37 ± 0.19^{ABbc}
	H	65.36 ± 0.11^{Ba}	63.74 ± 0.19^{Bb}	65.74 ± 0.18^{Aa}	63.88 ± 0.36^{Cb}	63.48 ± 0.36^{Bb}
Crude ash	**T**	2.26 ± 0.06^{Ab}	2.56 ± 0.09^{Aab}	2.76 ± 0.18^{Aab}	2.39 ± 0.03^{Aab}	2.84 ± 0.18^{Aa}
	C	1.97 ± 0.09^{Ab}	2.67 ± 0.05^{Aa}	2.70 ± 0.06^{Aa}	2.65 ± 0.22^{Aa}	2.94 ± 0.15^{Aa}
	H	1.95 ± 0.09^{Ab}	2.55 ± 0.04^{Aa}	2.50 ± 0.20^{Aa}	2.36 ± 0.03^{Aab}	2.63 ± 0.17^{Aa}
Crude protein	**T**	20.35 ± 0.25^{Ba}	20.1 ± 0.15^{Aa}	19.46 ± 0.21^{ABa}	19.93 ± 0.26^{Ba}	19.60 ± 0.14^{Aa}
	C	21.37 ± 0.04^{Aa}	19.98 ± 0.05^{Ab}	18.51 ± 0.11^{Bc}	21.78 ± 0.58^{Aa}	20.12 ± 0.04^{Ab}
	H	20.30 ± 0.03^{Ba}	20.21 ± 0.05^{Aa}	19.56 ± 0.37^{Aa}	20.21 ± 0.38^{ABa}	19.76 ± 0.18^{Aa}
Crude fat	**T**	9.65 ± 0.04^{Cd}	10.73 ± 0.08^{Bb}	11.31 ± 0.12^{Aa}	10.22 ± 0.13^{Bc}	10.41 ± 0.02^{Cbc}
	C	12.14 ± 0.06^{Aa}	10.65 ± 0.04^{Bc}	11.65 ± 0.12^{Ab}	9.56 ± 0.12^{Cd}	11.72 ± 0.10^{Bb}
	H	11.58 ± 0.10^{Bc}	12.68 ± 0.04^{Ab}	11.32 ± 0.13^{Ac}	12.61 ± 0.08^{Ab}	13.18 ± 0.17^{Aa}

Mean ($n = 6$) ± SD. A, B, C (↓): Different uppercase superscript letters within the same column indicate significant differences between groups ($p < 0.05$). a, b, c … f (→): Different lowercase superscript letters within the same row indicate significant differences between days ($p < 0.05$)

The observed regional differences in spoilage kinetics can be explained, at least in part, by compositional and structural variations among the anatomical segments. As detailed in Table 2, the center (C) region exhibited the highest initial protein content. This elevated protein level likely provides a stronger buffering capacity, thereby retarding pH shifts and contributing to the relatively slower spoilage progression observed in this group. In contrast, the head (H) region was characterized by higher lipid content. Since lipids are highly susceptible to oxidation, this composition may accelerate sensory deterioration and facilitate microbial proliferation. The tail (T) region, characterized by more active musculature and higher metabolic activity, displayed the fastest protein degradation and volatile nitrogen accumulation, a finding consistent with its elevated microbial counts recorded for this section. Furthermore, the richer vascularization and blood supply of the head region could facilitate microbial proliferation compared to the more homogeneous structure of the center fillets. Collectively, these compositional and physiological disparities provide a plausible explanation for the observed region-specific decay rates, underscoring the importance of analyzing anatomical sub-regions when evaluating spoilage dynamics in rainbow trout.

Beyond compositional variation, the observed divergence among the head, center, and tail regions can be mechanistically explained by the differential activity of coupled biochemical and microbial pathways across the fillet. First, lipid oxidation is expected to proceed faster in lipid-richer areas (e.g., near the head and darker muscle), where myoglobin/hemoglobin-bound iron catalyzes peroxidation of PUFA-rich phospholipids, yielding volatile aldehydes (e.g., hexanal), which drive early odor decline and color dulling; recent reviews detail heme-mediated catalysis in muscle foods and its sensory consequences (Dragoev, 2024; Wu et al., 2024). Second, proteolysis and deamination driven by specific spoilage organisms (SSOs) and endogenous proteases are accelerated in regions with lower effective buffering capacity and higher metabolic activity, such as the white muscle of the tail. This activity intensifies TVB-N formation (ammonia and amines) and causes a concomitant pH rise—biochemical shifts that are effectively detected by the pH-responsive intelligent label (ΔE). This mechanism is fully consistent with our TVB-N results, which showed the most rapid accumulation in the tail region, accompanied by a concurrent pH elevation and an earlier color transition in labels ($\Delta E > 5$). Contemporary syntheses link these amino acid catabolic routes and their temporal succession with spoilage progression in chilled fish (Chi et al., 2025; Wang & Zheng, 2025). Furthermore, the earlier and steeper rise in headspace CO_2 detected in the head and tail segments supports the hypothesis of microenvironmental differences accelerating microbial respiration in these specific areas. The CO_2 trajectory closely mirrored the sensory rejection points and the colorimetric behavior of the labels, reinforcing the mechanistic interpretation of region-specific deterioration. Collectively, these relationships confirm that the biochemical pathways underlying oxidation, proteolysis, and microbial activity are directly reflected in the measured patterns of TVB-N, CO_2, pH, microbial load, and label color change (ΔE).

Finally, intra-fillet heterogeneity regarding lipid distribution and fatty-acid profile (e.g., dark vs. light muscle; proximity to skin and vasculature) provides the structural basis for these pathways. This heterogeneity explains why the head samples exhibited earlier sensory signs of oxidation, whereas the tail samples displayed accelerated trajectories for TVB-N, pH, and CO_2. Spatial analyses of salmonids have reported non-uniform fatty-acid deposition across fillets, which aligns with our region-dependent kinetics (Patel et al., 2025). In conclusion, these interconnected mechanisms—heme-catalyzed lipid oxidation leading to sensory deterioration (odor and color) and microbial proteolysis causing TVB-N and pH increases (and thus label ΔE shifts)—provide a robust biochemical rationale for the region-specific correlations observed in the dataset.

Correlation of Intelligent Label Color Change with pH, TVB-N, CO2, Microbiological, and Sensory Changes

To evaluate the accuracy of the sensor array and confirm spoilage over time, a comprehensive monitoring approach was employed. This included physical, chemical, and microbiological analyses (TVB-N, pH, CO_2, total mesophilic aerobic bacteria (TMAB), total psychrophilic aerobic bacteria (TPAB), total coliforms (TC), total molds and yeasts (TMY), lactic acid bacteria (LAB), and *Pseudomonas* spp.), as well as sensory evaluation on both raw and cooked samples. The results obtained from these conventional methods were compared with the visual color changes of the intelligent labels. Given that the colorimetric response (ΔE) of the labels is triggered by the pH-sensitive anthocyanins incorporated into the polymer matrix, potential linear correlations were explored between label color change and the corresponding changes in headspace CO_2 concentration, total volatile basic nitrogen accumulation, pH variation, and microbial growth.

Sensory scores and total mesophilic and psychrophilic bacteria count (TMAB-TPAB) are widely recognized and reliable indicators for assessing the freshness of aquatic products.

In the T and H groups, the strongest positive correlations were observed between ΔE values and total psychrophilic aerobic bacteria (TPAB) counts, with correlation coefficients of $r = 0.977$ and $r = 0.974$, respectively.

At the aggregate level, TPAB counts tracked ΔE closely, supporting label's value as a general spoilage indicator. In

organism-specific analyses, ΔE correlated significantly with both *Pseudomonas* spp. and LAB, although the patterns differed across anatomical regions. In the tail (T) group, the highest correlation with ΔE was observed for *Pseudomonas* ($r = 0.883$), whereas in the center (C) and head (H) groups, the strongest correlations were observed for LAB ($r = 0.868$ and 0.874, respectively). Notably, LAB–ΔE correlations were highly consistent across regions, while *Pseudomonas*–ΔE correlations varied more notably (C: 0.799, H: 0.820 vs. T: 0.883). In our data, LAB counts exceeded *Pseudomonas* counts in all groups, and the rise of headspace CO_2 during storage paralleled the LAB growth trajectory more closely than that of *Pseudomonas*. This observation is consistent with reports that CO_2-enriched atmospheres inhibit Gram-negative aerobes such as *Pseudomonas* (Yousefi et al., 2019), while moderate CO_2 levels can favor the competitiveness of LAB under chilled conditions (Yingyuad et al., 2006). The stronger correlations in the center and head LAB groups may also reflect the higher blood content in these regions, which facilitates microbial growth. Collectively, these findings suggest that the intelligent labels effectively captured the dominant spoilage trajectories in each region, while the ecological interplay between microbial succession and package atmosphere likely shaped the observed patterns.

Similar associations between psychrophilic bacteria, particularly *Pseudomonas* spp. and LAB, and spoilage progression in cold-stored rainbow trout have been highlighted in recent studies (Wang et al., 2025a).

Conversely, the strongest negative correlations were identified between label color shifts and sensory attributes. In the T group, a strong negative correlation was observed with the odor scores of cooked samples ($r = -0.972$), while in the H group, the most pronounced negative correlation was with the flavor scores ($r = -0.984$). In the C group, the ΔE values exhibited the highest positive correlation with headspace CO_2 concentration ($r = 0.977$), while the strongest negative correlation was found with the texture scores of fresh samples ($r = -0.961$). Consistent with these relationships, panelists began to detect unpleasant odors in T and H samples starting from day 7, which coincided with a marked decline in odor scores. Concurrently, psychrophilic bacterial counts exceeded 4 log CFU/g from day 6 onward in both groups, paralleling the label's transition to pinkish hues (Fig. 3). This indicates that the color changes intelligent labels were closely aligned with psychrophilic bacterial growth and odor deterioration, thereby serving as an effective early spoilage indicator. The strong correspondence between ΔE and sensory rejection scores demonstrates

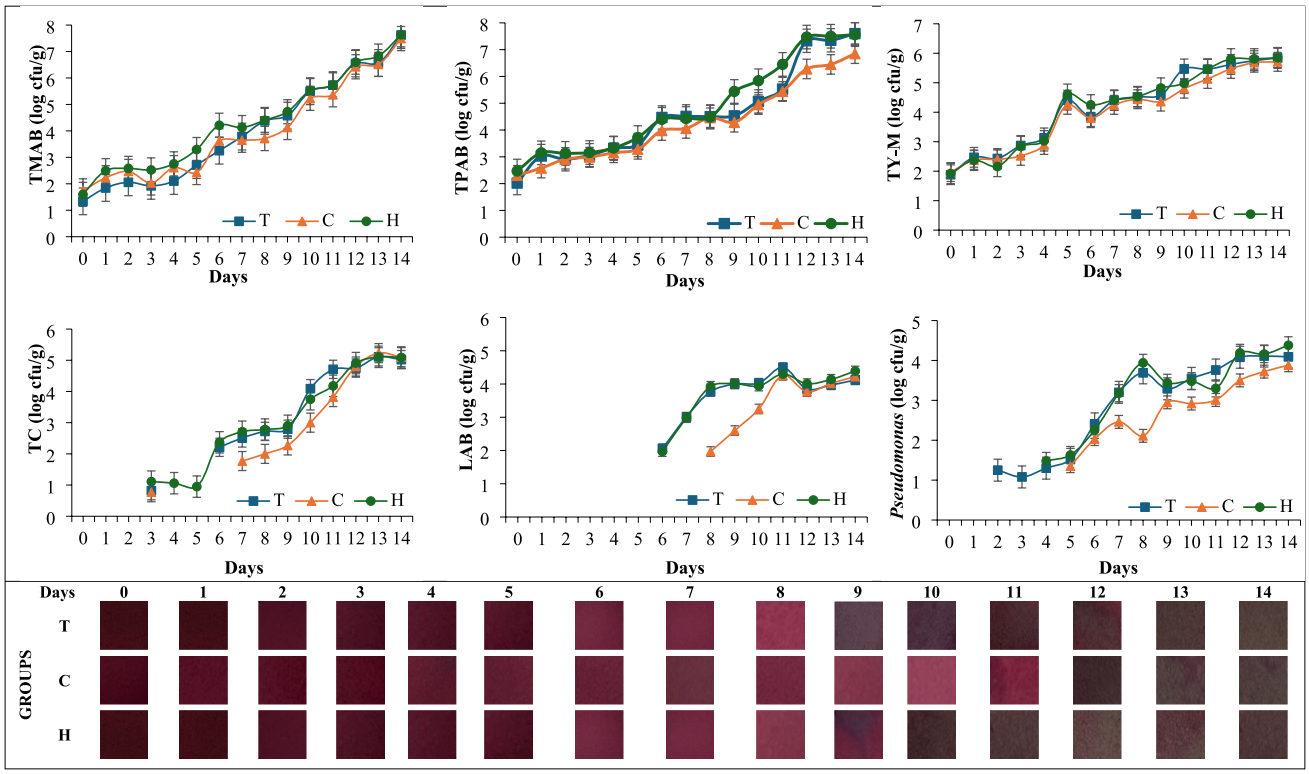

Fig. 3 Microbiological spoilage indicators and corresponding color responses of intelligent labels during refrigerated storage ($n = 4$). Total mesophilic aerobic bacteria (TMAB), total psychrophilic aerobic bacteria (TPAB), total yeast and mold (TY-M), total coliforms (TC), lactic acid bacteria (LAB), and *Pseudomonas* spp. counts are presented along with the visual appearance of intelligent labels on each sampling day

that label color change mirrors consumer-perceived freshness loss, reinforcing the label's practical interpretability. Despite anatomical heterogeneity across the head, center, and tail regions, ΔE maintained robust relationships with spoilage indicators, enabling region-specific deterioration to be captured by a single, observable color metric.

Microbiological results for the experimental groups across different storage periods are presented in Fig. 3. On day 0, the TMAB counts were 1.34 ± 0.11, 1.73 ± 0.05, and 1.60 ± 0.02 log CFU/g for the T, C, and H groups, respectively. A significant increase ($p < 0.05$) in TMAB counts was observed in all samples throughout the storage period. According to the International Commission on Microbiological Specifications for Foods (ICMSF, 1986), a microbial load of 7 log CFU/g is considered the upper acceptability limit for fish. Similarly, Aghaei et al. (2020) reported that the total bacterial load in rainbow trout increased from an initial level of 0.85 to 2.66 log CFU/g by day 6 and reached 7.15 log CFU/g after the 12th day of storage. In the present study, no noticeable color change was observed in the intelligent labels during the first 4 days under refrigerated conditions; however, a light purple hue became discernible on day 6. This aligns with observations in previous studies noting a temporal lag between reaching microbial thresholds and the detection of TVB-N. This discrepancy is attributed to the fact that the production of volatile bases is a secondary process that follows the exponential growth of microbial populations. Specifically, specific spoilage microorganisms (SSOs) are initially present in low numbers but proliferate rapidly over time, subsequently generating the metabolites responsible for undesirable changes in odor, flavor, color, and texture (Huang et al., 2019).

Initial, TPAB counts (day 0) were 2.02 ± 0.07, 2.31 ± 0.06, and 2.47 ± 0.09 log CFU/g for the T, C, and H groups, respectively. A significant increase ($p < 0.05$) in TPAB counts was observed in all samples throughout the storage period. Psychrophilic bacteria are widely recognized as the primary contributors to quality degradation in fish under refrigerated storage conditions (Ojagh et al., 2010). Consistent with these findings, Aghaei et al. (2020) reported that the total bacterial load in rainbow trout increased from an initial level of 0.85 to 2.66 log CFU/g by day 6, reaching 7.15 log CFU/g after the 12th day of storage. Similarly, Wells et al. (2019), using a colorimetric film indicator at 4 °C and 22 °C, demonstrated a strong correlation between color changes and microbial colony formation. Furthermore, Forghani et al. (2023) also observed a very strong correlation between ΔE values in both TPAB ($R^2 = 0.9918$) and TMAB ($R^2 = 0.9632$) counts in shrimp samples when evaluating the effectiveness of intelligent labels.

Although yeast and mold counts increased during storage, they remained below the established spoilage threshold of 6 log CFU/g. Peleg (2022) noted that yeasts and molds typically become dominant under conditions of reduced water activity. However, in the present study, the progressive decline in water activity—attributed to cellular degradation and moisture loss driven by microbial and enzymatic activity—may have limited their proliferation during the later stages of storage.

In a related study, Uçak and Elsheıkh (2023) reported that the initial coliform count in seabass fillets was 1.8 log CFU/g. This value increased progressively during storage under atmospheric packaging, reaching 5.47 log CFU/g by the end of shelf life.

Regarding lactic acid bacteria (LAB), counts remained below 0.30 log CFU/g until day 6 in the T and H groups and until day 8 in the C group. The production of lactic acids and bacteriocins by LAB is known to inhibit the growth of competing microbiota, thereby facilitating their selective proliferation during seafood spoilage (Sharma et al., 2022). In the present study, a stagnation in total coliform growth was observed on days when LAB counts exceeded 4 log CFU/g, suggesting that LAB proliferation may have suppressed the coliform population. Furthermore, toward the end of the storage period, the accumulation of headspace CO_2 likely exerted an inhibitory effect on LAB growth itself. Similarly, Pournis et al. (2005) reported that elevated CO_2 concentrations in modified atmosphere packaging (MAP) of red mullet (*Mullus surmuletus*) significantly inhibited LAB activity. Conversely, Françoise (2010) noted that LAB generally demonstrate limited effectiveness in fresh seafood stored under aerobic or anaerobic conditions, being more active in processed products such as marinated, salted, or cold-smoked fish.

Initial *Pseudomonas* spp. counts were below the detection limit (< 0.30 log CFU/g) in all groups. Bacterial levels remained suppressed in the T, C, and H groups until days 2, 5, and 4, respectively, likely attributable to rapid post-harvest processing and effective chilled transport. A significant increase in *Pseudomonas* spp. counts was recorded in all groups throughout storage ($p < 0.05$), with the highest value observed in the H group on day 14 (4.38 log CFU/g). A marked acceleration in growth occurred between days 4 and 8 across all groups (Fig. 3), and significant inter-group differences were observed on days 8 and 14 ($p < 0.05$). These results align with previous studies identifying *Pseudomonas* spp. as the primary psychrophilic aerobic spoilage agents in refrigerated fish (Luo et al., 2023; Moradi et al., 2019). Although growth rates decrease at refrigeration temperatures, psychrophilic *Pseudomonas* spp. can still proliferate at low temperatures and produce spoilage-related metabolites (e.g., VOCs, biogenic amines, TMA), contributing to seafood spoilage (Wang et al., 2025a).

However, as storage progressed, the accumulation of headspace CO_2 likely exerted an inhibitory effect on *Pseudomonas* spp. growth, particularly after day 9. Similar trends

have been reported in studies using modified atmosphere packaging (Yousefi et al., 2019), where elevated CO_2 levels were shown to suppress aerobic spoilage bacteria. While quantitative differences between studies may be attributed to variations in fish species and specific packaging conditions, the underlying inhibitory mechanism is consistent. Overall, ΔE demonstrated a robust relationship with microbial proliferation. Crucially, the onset of distinct color transitions corresponded to microbial loads approaching rejection thresholds, thereby confirming the label's microbiological relevance.

The increase in microbial load leads to the production of volatile compounds such as carbon dioxide, ammonia, dimethylamine, and trimethylamine, which accumulate in the package headspace. Therefore, pH-sensitive indicators serve as effective tools for tracking food spoilage over time (Hassanpour et al., 2022; Morsy et al., 2016). In the C group, headspace CO_2 accumulation—driven by microbial activity—exhibited a strong correlation with label color change ($r = 0.977$). The second strongest correlation in this group was observed between ΔE and the texture scores of fresh samples, as well as the muscle structure scores of cooked samples. This suggests that elevated CO_2 levels may have contributed to the observed texture changes. While CO_2 can inhibit certain microbial populations like coliforms, its excessive accumulation can negatively impact product quality by altering muscle texture. In the H group, it is likely that the dissolution of CO_2 into water formed carbonic acid, which led to textural firming and a slightly sour taste, contributing to the lower texture and structure scores assigned by the panelists. This hypothesis is supported by the pH data for the H group, where values remained near baseline levels even on day 10 despite progressing microbial spoilage, whereas texture scores declined sharply after this point. Lannelongue et al. (1982) reported a similar phenomenon in shrimp packed under atmospheric air, where CO_2 concentrations reached 20% by day 10 primarily due to microbial respiration. Ultimately, the alignment between headspace CO_2 accumulation and label color transitions supports the effectiveness of headspace-mounted labels in reflecting intensified microbial activity and progressing spoilage.

The correlation coefficients between pH values and label color changes (ΔE) for the T, C, and H groups were $r = 0.885$, $r = 0.821$, and $r = 0.911$, respectively. Initially, the indicator labels appeared red on fresh samples. No significant color deviation was observed until pH levels approached 6.9, at which point a subtle pinkish shift became discernible. During storage, the pH of the fish samples rose gradually from 6.30 to 7.40, a range consistent with values reported by Gandotra et al. (2012). Visually detectable color transitions emerged after day 8 in the T group, day 9 in the H group, and day 12 in the C group. As spoilage advanced and the pH neared 7.4, the labels transitioned from red to pink, subsequently shifting to grayish-brown and finally to green hues. Collectively, the progressive rise in pH exhibited a strong positive correlation with ΔE, confirming that the label color effectively mirrored the alkaline shift driven by microbial spoilage.

TVB-N levels, a critical determinant of fish quality, exhibited strong positive correlations with ΔE values in the T, C, and H groups ($r = 0.930$, 0.922, and 0.916, respectively). Given the high sensitivity of anthocyanin-based indicators to ammonia, a rapid response to TVB-N accumulation was anticipated, particularly during the early-to-mid stages of spoilage. In this study, the indicators initially appeared dark red but gradually shifted to pink, coinciding with marked TVB-N increases recorded on days 7, 9, and 8 for the T, C, and H groups, respectively. The corresponding ΔE values were 7.44, 6.87, and 9.08. This pink coloration indicated that the samples were approaching the limit of acceptable freshness. TVB-N accumulates primarily due to microbial and enzymatic degradation of proteins, often occurring alongside CO_2 production. Various studies have proposed rejection thresholds for fish products ranging from 20 to 35 mg/100 g (Forghani et al., 2023). Specifically, Nowzari et al. (2013) identified 25 mg/100 g as the critical level marking the onset of spoilage, while Bekhit et al. (2021) suggested a stricter critical range of 15–25 mg/100 g. Consistent with these findings, Forghani et al. (2023) reported a strong correlation ($r = 0.8653$) between TVB-N accumulation and label color shifts in shrimp. In the present study, the increase in ΔE closely tracked TVB-N kinetics, with distinct color transitions aligning with established spoilage limits, thereby underscoring the label's utility as a chemical freshness indicator.

Overall, the correlation analysis demonstrated robust and consistent relationships between ΔE values and key spoilage indicators (pH, TVB-N, headspace CO_2, microbial counts, and sensory scores), confirming the reliability of the colorimetric response for the real-time assessment of fish freshness.

Sensory Analysis

As illustrated in Fig. 4, sensory scores for both raw and cooked samples were evaluated throughout the storage period to monitor quality deterioration. Sensory evaluation is considered one of the primary and reliable quality control methods used to assess the freshness and overall quality of food products (Esteves & Aníbal, 2021). At the onset of storage, all fresh sample groups exhibited firm texture, a shiny surface, and an overall appealing appearance. Regarding appearance, statistically significant differences among groups were only observed on days 5 and 11 ($p < 0.05$). This finding was supported by the noticeable color difference detected on day 6 ($\Delta E = 5.39$), indicating visible

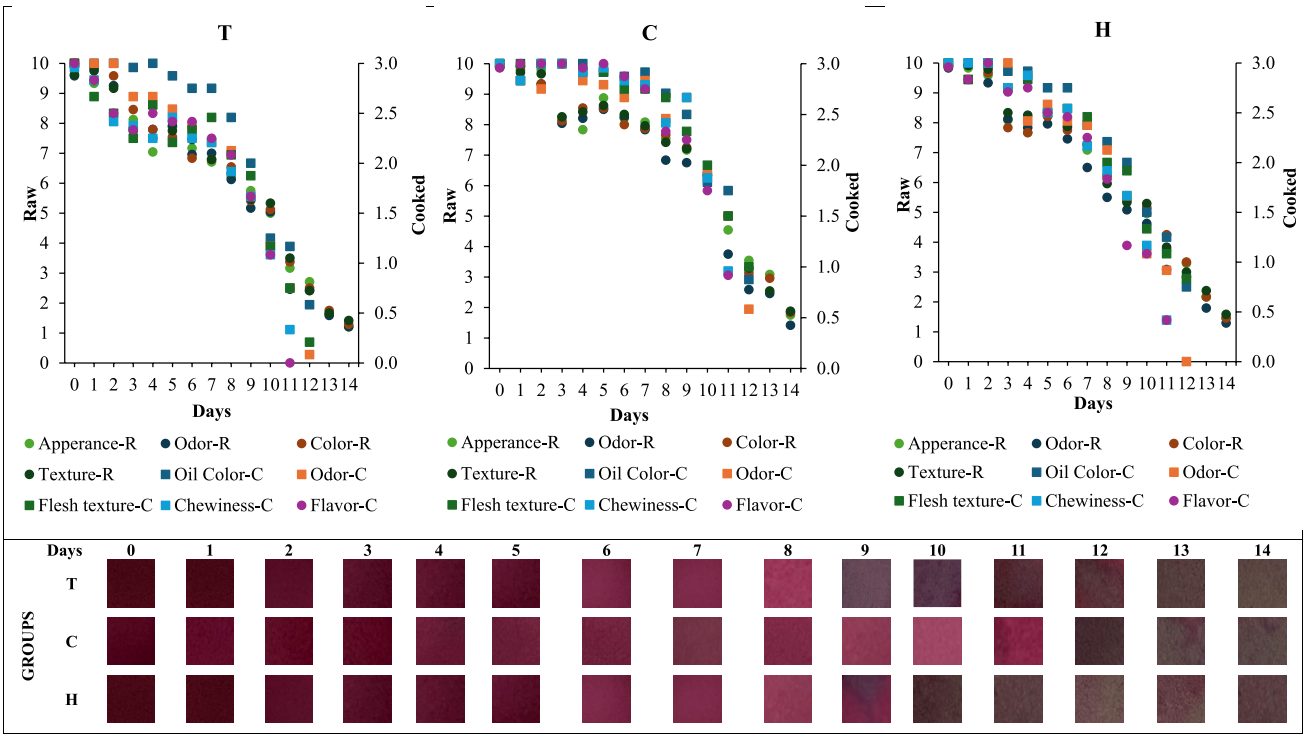

Fig. 4 Changes in sensory evaluation scores (R, raw samples; C, cooked samples) of fish fillet portions (T, tail-end; C, center; H, head-end) during refrigerated storage and representative color changes of intelligent labels during the storage of rainbow trout fillets at 4 ± 1 °C. The labels exhibited a gradual color shift corresponding to storage time: initially red/pink on day 0, lost color intensity (dark red intensity decreased) by day 6, shifting to greenish/brownish-green by day 12 and dark brownish-green by day 14, reflecting progressive spoilage

discoloration in fish muscle. Throughout storage, the decline in appearance scores of raw fish samples reflected the progressive loss of quality, with the T group exhibiting more rapid deterioration compared to the C and H groups. During the first 9 days, all groups maintained appearance scores above 5; however, a marked decline ensued after day 10. Correspondingly, the odor scores for the T group fell below the acceptable threshold of 3 on day 11, whereas the C and H groups dropped below this limit starting from day 12. These low odor scores coincided with the visual transition of the intelligent labels from pinkish hues to brownish-green tones. The odor evaluation results obtained in this study align with findings reported by Cardinal et al. (2006).

Meat color is a key quality indicator for consumers, complementing various biochemical parameters (Sánchez et al., 2023). As shown in Fig. 4, color scores for all groups remained above the acceptability threshold during the first 10 days of storage; however, a significant decline was observed from day 11 onward ($p < 0.05$). On day 12, the color scores of the T group dropped below the acceptable limit of 3, followed by the C and H groups on day 13. The distinct coloration of rainbow trout is largely due to astaxanthin, a dietary additive commonly used in aquaculture to enhance nutritional and sensory attributes (Bjørklund et al., 2022). The antioxidant nature of astaxanthin likely delayed visual quality deterioration during the early storage phase. A similar downward trend was observed in texture scores, which closely mirrored the decline in color ratings. Significant differences among groups on days 12 and 13 ($p < 0.05$) support the conclusion that both color and texture are reliable indicators of spoilage progression.

Regarding the sensory evaluation of oil color in cooked samples, no statistically significant differences ($p > 0.05$) were observed among the groups until day 7. During this period, all samples received scores equal to or above 2.7, corresponding to the reddish-pink hues observed on the intelligent labels, indicating a "very good" quality level. From day 9 onwards, the oils released during cooking began to exhibit browning, gradually losing their initial clarity and becoming opaque. Consequently, the oil color scores for the T, C, and H groups declined sharply, falling below the acceptable limit of 1 by day 12. These findings indicate that while all groups maintained comparable performance in terms of oil color up to day 7, a noticeable deterioration commenced after day 9.

Concurrently, a sharp decline in odor scores for cooked fish samples was observed in the T and H groups starting on day 8, coinciding with the emergence of visible spoilage symptoms. Odor scores for the T and H groups dropped below the acceptability threshold (score = 1) by day 11,

whereas the C group reached this limit on day 12. This indicates that the C group retained superior sensory quality with respect to odor for a longer period than the other groups. As noted by Huang et al. (2019), spoilage-associated off-odors result from the proliferation of specific spoilage organisms (SSOs). These organisms, initially present in low numbers, proliferate rapidly over time, generating metabolites responsible for undesirable shifts in odor, flavor, color, and texture.

Regarding chewiness, marked reductions in sensory scores were recorded in the T and H groups from day 7 onwards, attributed to a loss of juiciness and elasticity, accompanied by a mushy appearance. Similar textural degradation was observed in the C group starting on day 9. Although fat color, odor, and tissue structure assessments were conducted until day 12, panelists refused to perform the chewiness test on day 12 due to the samples being deemed unacceptable. This rejection was based on the fact that multiple sensory attributes had already fallen below their defined spoilage thresholds: flavor scores of cooked samples dropped below 1 in all groups by day 11, oil color scores declined below 1 on day 12, odor scores fell below 1 in the T and H groups on day 11 and in the C group on day 12, and chewiness scores had already decreased to below 1 in all groups by day 11. Collectively, the simultaneous deterioration of flavor, odor, oil color, and chewiness confirmed that the samples had exceeded the spoilage threshold, thereby justifying the termination of sensory tasting panels on day 12.

Visually detectable color changes in the intelligent labels were first observed on day 6, most notably in the tail and head groups. At this stage, odor scores for raw samples had declined from the "liked" to the "moderately liked" category, signaling the onset of perceptible quality loss while remaining above the rejection threshold. As storage progressed, odor scores for cooked samples in the T and H groups dropped below the spoilage threshold on day 11 (and day 12 for the C group), coinciding with the label's color shift to brownish-green. By day 12, when both cooked oil color and chewiness scores fell below 1 in all groups, the labels had already exhibited their most distinct color transition. This progression demonstrates that the label's color transitions are closely aligned not only with gradual sensory quality decline but also with critical rejection points, underlining their practical value as real-time freshness indicators.

The freshness classifications presented in Fig. 5 were established based on overall sensory scores, representing the average ratings across multiple criteria rather than a single attribute. For raw fillets, mean scores derived from the combined evaluation of appearance, odor, color, and texture were utilized; values ≥ 8 were assumed to represent the Fresh category, whereas values < 4 were considered to indicate the spoilage threshold. For cooked fillets, the combined evaluation of oil color, odor, flesh texture, chewing characteristics, and flavor was applied; mean scores ≥ 2.5 were assumed to represent the Fresh category, while scores < 1.5 were considered as the spoilage threshold. Intermediate mean values in both cases were classified as "OK" (acceptable, edible). For each anatomical region (T, C, H), the specific days on which these sensory limits were reached were identified. Consequently, the corresponding values of Δ*E*, TVB-N,

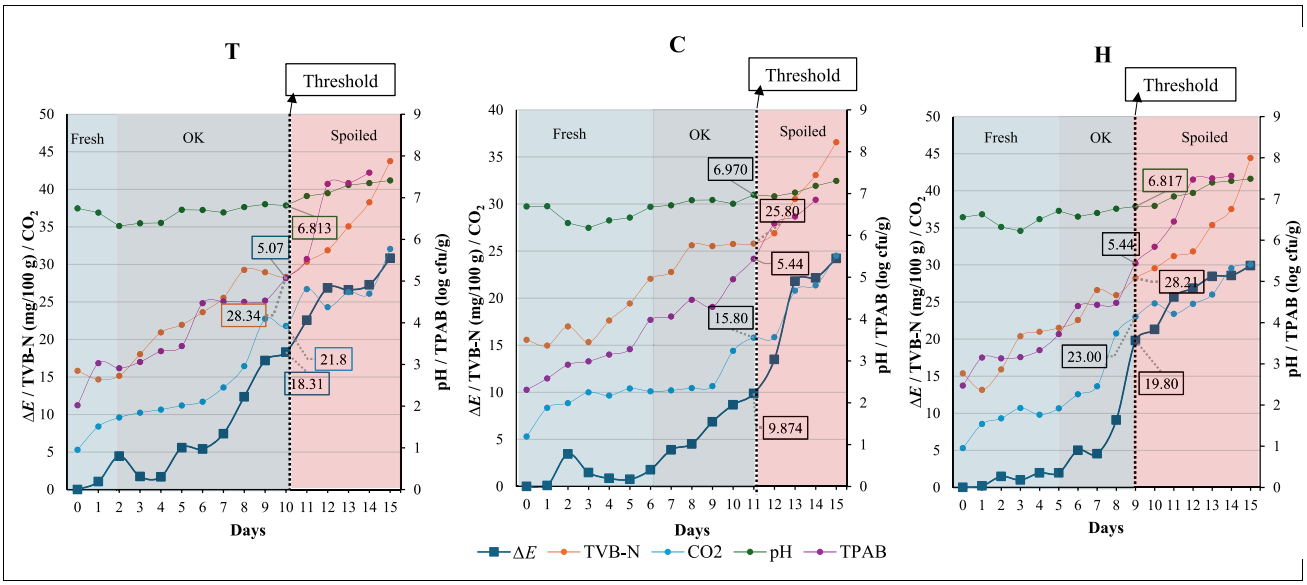

Fig. 5 Determination of spoilage progression, Δ*E*, TVB-N, pH, CO_2, and TPAB thresholds and freshness classification of rainbow trout fillets (tail, center, head) during refrigerated storage based on sensory evaluation (raw sample mean sensory scores: ≥ 8 fresh, < 4 spoilage threshold; cooked sample mean sensory scores: ≥ 2.5 fresh, < 1.5 spoilage threshold)

in-pack CO_2, pH, and TPAB recorded on those days were regarded as empirical reference thresholds. This approach was aimed at aligning instrumental and microbiological indicators with consumer-relevant sensory limits derived from multiple evaluation criteria, thereby providing a more integrated framework for interpreting spoilage progression across fish regions.

Anthocyanin-based intelligent labels may offer a practical cue for seafood freshness by visualizing region-specific spoilage patterns. Their potential contribution to reducing waste should be regarded as context-dependent and subject to pilot-scale validation (e.g., stability, unit cost, and integration with routine stock rotation/markdown practices). Within these constraints, such labels could help earlier identification and handling of at-risk lots, thereby potentially supporting more efficient inventory decisions. Similar reviews have emphasized that intelligent packaging systems can substantially contribute to food waste reduction by facilitating real-time quality monitoring, enabling dynamic pricing or inventory rotation, and guiding consumer purchasing decisions (Ganeson et al., 2023; Abekoon et al., 2024; Kahyaoglu, 2024).

Conclusion

This study establishes that POPAS-based intelligent labels serve as effective, non-invasive, and responsive indicators for real-time monitoring of freshness and spoilage progression in rainbow trout fillets during refrigerated storage. A key contribution of this study is the demonstration that POPAS-based intelligent labels effectively track spoilage progression and accurately reflect sensory rejection points, with the added novelty of revealing region-specific spoilage patterns across the head, center, and tail portions of the fillet. The labels showed strong alignment with sensory rejection points, as well as with microbial, chemical, and physicochemical spoilage markers. These findings highlight the potential of POPAS-based labels to serve as practical, consumer-friendly freshness indicators and to support improved cold-chain management practices.

In addition to their analytical performance, the labels offer opportunities for integration into sustainable intelligent packaging systems, addressing both food safety needs and growing environmental concerns associated with synthetic indicators. Nevertheless, further research is needed to enhance their practical applicability. Future studies should examine label stability under different packaging atmospheres (e.g., vacuum, MAP), evaluate performance in other fish and seafood species, and validate the technology under real supply-chain conditions. Additional efforts involving mechanical durability, large-scale manufacturing, and consumer perception studies will be essential for advancing industrial adoption and commercial readiness. Together, these directions may broaden the applicability of anthocyanin-based indicators and strengthen their role in ensuring quality and safety in seafood products.

Acknowledgements This manuscript was composed of a doctorate dissertation entitled: "Investigation of the Use of pH Sensitive Smart Label Developed Using Purple Onion (*Allium cepa* L.) Peel in Determining the Quality of Rainbow Trout (*Oncorhynchus mykiss*) Stored Under Cold Storage Conditions" (National Thesis No. 873528) in Sinop University, Institute of Science, in 2024. This study was supported by Sinop University Scientific Research Coordination Unit. Project Number: SÜF-1901-23-001, 2024. Also, Bayram Köstekli is thankful to the Scientific and Technological Research Council of Turkey (TUBITAK-2211-A National Ph.D. program) and the YOK 100-2000 Ph.D. scholarship program for financial support.

Author Contributions All authors' contributions are as follows: B.K.: Conceptualization, Data curation, Formal analysis (equal), Investigation, Methodology, Writing-original draft, writing–review and editing, Visualization. M.E.E: Funding acquisition, Project administration, Supervision, Validation. C.O.A: Formal analysis (equal). B.Ç: formal analysis (equal). R.K: formal analysis (equal). All authors reviewed the manuscript.

Funding This study was supported by Sinop University Scientific Research Coordination Unit. Project Number: SÜF-1901–23-001, 2024.

Data Availability The data that support the findings of this study are available on request from the corresponding author. The data are not publicly available due to privacy or ethical restrictions.

Declarations

Competing interests The authors declare no competing interests.

References

Abekoon, T., Buthpitiya, B. L. S. K., Sajindra, H., Samarakoon, E. R. J., Jayakody, J. A. D. C. A., Kantamaneni, K., & Rathnayake, U. (2024). A comprehensive review to evaluate the synergy of intelligent food packaging with modern food technology and artificial intelligence field. *Discover Sustainability, 5*(1), 160. https://doi.org/10.1007/s43621-024-00371-7

Aghaei, Z., Ghorani, B., Emadzadeh, B., Kadkhodaee, R., & Tucker, N. (2020). Protein- based halochromic electrospun nanosensor for monitoring trout fish freshness. *Food Control, 111*, Article 107065. https://doi.org/10.1016/j.foodcont.2019.107065

Akbari, S. M., & Mehregan Nikoo, A. (2025). Fabrication of pH-sensitive smart indicator film from polylactic acid and elderberry anthocyanin for monitoring chicken spoilage. *Packaging Technology and Science, 38*, 640–659. https://doi.org/10.1002/pts.2897

Almasi, H., Forghani, S., & Moradi, M. (2022). Recent advances on intelligent food freshness indicators; An update on natural colorants and methods of preparation. *Food Packaging and Shelf Life, 32*, Article 100839. https://doi.org/10.1016/j.fpsl.2022.100839

AOAC. (1995). Official methods of analysis. Association of official analytical chemists, *Gaithersburg, MD, USA*.

AOAC. (2000). *Official methods of analysis* (17th ed.). Association of Official Analytical Chemists.

AOAC. (2005). Official methods of analysis of AOAC International (18th ed.). *Gaithersburg, MD, USA*.

Basdeki, E., Vasilaki, S. E., Sensi, M., Flemetakis, E., Biscarini, F., Power, D., & Tsironi, T. (2025). Reviewing the correlation of fish quality alteration and in-package headspace composition: Evidence from a pH freshness indicator case study. *International Journal of Food Science, 2025*(1), 3576183. https://doi.org/10.1155/ijfo/3576183

Bekhit, A. E. D. A., Holman, B. W., Giteru, S. G., & Hopkins, D. L. (2021). Total volatile basic nitrogen (TVB-N) and its role in meat spoilage: A review. *Trends in Food Science & Technology, 109*, 280–302. https://doi.org/10.1016/j.tifs.2021.01.006

Bjørklund, G., Gasmi, A., Lenchyk, L., Shanaida, M., Zafar, S., Mujawdiya, P. K., Lysiuk, R., Antonyak, H., Noor, S., Akram, M., Smetanina, K., Piscopo, S., Upyr, T., & Peana, M. (2022). The role of astaxanthin as a nutraceutical in health and age-related conditions. *Molecules, 27*(21), Article 7167. https://doi.org/10.3390/molecules27217167

Boccalon, E., Sassi, P., Pioppi, L., Ricci, A., Marinozzi, M., Gorrasi, G., & Nocchetti, M. (2022). Onion skin extract immobilized on Halloysite-layered double hydroxide filler as active pH indicator for food packaging. *Applied Clay Science, 227*, Article 106592. https://doi.org/10.1016/j.clay.2022.106592

Brown, V. I., & Lowbury, E. J. L. (1965). Use of improved cetrimide agar medium ad other culture methods for *Pseudomonas aureginosa*. *Journal of Clinical Pathology, 18*, 752–756.

Cardinal, M., Cornet, J., Serot, T., & Baron, R. (2006). Effects of the smoking process on odour characteristics of smoked herring (*Clupea harengus*) and relationships with phenolic compound content. *Food Chemistry, 96*, 137–146. https://doi.org/10.1016/j.foodchem.2005.02.040

Chen, S., Li, Z., Ren, D., Wu, X., & Xu, D. (2025). Improved sensitivity of freshness indicator based on purple sweet potato anthocyanins through pH optimization and its application in flesh food monitoring during logistics. *Innovative Food Science & Emerging Technologies, 100*, Article 103929. https://doi.org/10.1016/j.ifset.2025.103929

Chi, Y., Luo, M., & Ding, C. (2025). The role of microbiota in fish spoilage: Biochemical mechanisms and innovative preservation strategies. *Antonie Van Leeuwenhoek, 118*(7), 89. https://doi.org/10.1007/s10482-025-02101-z

Choi, I., Lee, Y. J., Lacroix, M., & Han, J. (2017). Intelligent pH indicator film composed of agar/potato starch and anthocyanin extracts from purple sweet potato. *Food Chemistry, 218*, 122–128. https://doi.org/10.1016/j.foodchem.2016.09.05

Dai, W., Yin, P., Lin, Q., Tian, M., Wu, M., Ding, J., & Fang, Y. (2025). Black goji anthocyanin-loaded emulsion film stabilized by rice protein hydrolysate complexes as pH-sensitive indicator for salmon freshness. *Food Packaging and Shelf Life, 47*, Article 101419. https://doi.org/10.1016/j.fpsl.2024.101419

Devi, D., Kumar, S., & Mukherjee, A. (2024). Onion peel extract as milk freshness indicator in biopolymer-based intelligent packaging films. *Food and Humanity, 2*, Article 100223. https://doi.org/10.1016/j.foohum.2023.100223

Dragoev, S. G. (2024). Lipid peroxidation in muscle foods: Impact on quality, safety and human health. *Foods, 13*(5), Article 797. https://doi.org/10.3390/foods13050797

Esmaeili, K., Golshahi, H., Dashtian, K., & Zare-Dorabei, R. (2025). An innovative hydrogel-based colorimetric freshness indicator array for smart packaging of bananas, apples, and pears. *Sensors and Actuators B: Chemical, 438*, Article 137743. https://doi.org/10.1016/j.snb.2025.137743

Esteves, E., & Aníbal, J. (2021). Sensory evaluation of seafood freshness using the quality index method: A meta-analysis. *International Journal of Food Microbiology, 337*, Article 108934. https://doi.org/10.1016/j.ijfoodmicro.2020.108934

Ezati, P., & Rhim, J. W. (2020). pH-responsive chitosan-based film incorporated with alizarin for intelligent packaging applications. *Food Hydrocolloids, 102*, Article 105629. https://doi.org/10.1016/jfoodhyd.2019.105629

Far, B. F., Jahanbakhshi, M., Jameie, L., Shojaei, A., Zarei, K., Taromi, P., ..., Ertas, Y. N. (2025). Chitosan-graft-gelatin hydrogel containing bromothymol blue as a food spoilage indicator for intelligent food packaging. *Advanced Materials Interfaces*, *12*(9), 2400799. https://doi.org/10.1002/admi.202400799

Fatehi, F., Khalili Sadrabad, E., Feilizadeh, M., Derakhshan, Z., Heidari Kochaki, S., Hekmatimoghaddam, S., ..., Mohajeri, F. A. (2025). Designing the pH-sensitive indicator based on starch nanoparticle with bromocresol green for monitoring meat spoilage. *International Journal of Environmental Health Research*, *35*(5), 1204–1212. https://doi.org/10.1080/09603123.2024.2383427

Forghani, S., Zeynali, F., Almasi, H., & Hamishehkar, H. (2023). Accurate monitoring of shrimp freshness via cornflower anthocyanins-loaded bio-based nanofiber mats and casted films. *Journal of Polymers and the Environment, 31*(10), 4258–4273. https://doi.org/10.1007/s10924-023-02867-1

Françoise, L. (2010). Occurrence and role of lactic acid bacteria in seafood products. *Food Microbiology, 27*(6), 698-709. https://doi.org/10.1016/j.fm.2010.05.016

Gandotra, R., Sharma, S., Koul, M., & Gupta, S. (2012). Effect of chilling and freezing on fish muscle. *Journal of Pharmacy and Biological Sciences, 2*(5), 5–9.

Ganeson, K., Mouriya, G. K., Bhubalan, K., Razifah, M. R., Jasmine, R., Sowmiya, S., & Ramakrishna, S. (2023). Smart packaging– A pragmatic solution to approach sustainable food waste management. *Food Packaging and Shelf Life, 36*, Article 101044. https://doi.org/10.1016/j.fpsl.2023.101044

Ghanbarzadeh, B., Almasi, H., & Entezami, A. A. (2010). Physical properties of edible modified starch/carboxymethyl cellulose films. *Innovative Food Science & Emerging Technologies, 11*(4), 697–702. https://doi.org/10.1016/j.ifset.2010.06.001

Halkman, A. K. (2005). Gıda Mikrobiyolojisi ve Uygulamaları (p. 358). *Başak Matbaacılık. Ankara*, Türkiye.

Hardy, M., Moser, B., Haughey, S. A., & Elliott, C. T. (2024). Does the fish rot from the head? Hyperspectral imaging and machine learning for the evaluation of fish freshness. *Chemometrics and Intelligent Laboratory Systems, 245*, Article 105059. https://doi.org/10.1016/j.chemolab.2023.105059

Hassanpour, A., Moradi, M., Tajik, H., & Molaei, R. (2022). Development of two types of intelligent indicators based on cellulose, black carrot, and grape anthocyanins for monitoring food freshness/spoilage. *Journal of Food Measurement and Characterization, 16*(6), 4295–4302. https://doi.org/10.1007/s11694-022-01507-x

Hsiao, H. I., & Chang, J. N. (2017). Developing a microbial time–temperature indicator to monitor total volatile basic nitrogen change in chilled vacuum-packed grouper fillets. *Journal of Food Processing and Preservation, 41*(5), Article e13158. https://doi.org/10.1111/jfpp.13158

Huang, H., Zhou, G., Meng, Z., Li, T., Sun, L., Wang, Z., & Yang, Y. (2025). A novel flavonol-based self-assembled sensor with high sensitivity to biogenic amines and application in detection of fish and prawn freshness. *Food Control*, *180*, 111645. https://doi.org/10.1016/j.foodcont.2025.111645

Huang, S., Xiong, Y., Zou, Y., Dong, Q., Ding, F., Liu, X., & Li, H. (2019). A novel colorimetric indicator based on agar incorporated with *Arnebia euchroma* root extracts for monitoring fish freshness. *Food Hydrocolloids, 90*, 198–205. https://doi.org/10.1016/j.foodhyd.2018.12.009

Huang, Y. G., Wang, G. Y., Qi, K. X., Fang, P. F. (2021). Study on Freshness Indicator Agent of Natural Plant Dyes. In: Sun, X.,

Zhang, X., Xia, Z., Bertino, E. (eds) Advances in Artificial Intelligence and Security. *Communications in Computer and Information Science*, vol 1423. Springer, Cham. https://doi.org/10.1007/978-3-030-78618-2_44

ICMSF. (1986). International commission on microbiological specifications for foods. Sampling plans for fish and shellfish. In ICMSF (Ed.), Microorganisms in foods 2. *Sampling for microbiological analysis: principles and scientific applications* (Vol. 2, 2nd ed., pp. 181–196). Toronto Canda: University of Toronto Press.

Janjarasskul, T., & Suppakul, P. (2018). Active and intelligent packaging: The indication of quality and safety. *Critical Reviews in Food Science and Nutrition, 58*(5), 808–831. https://doi.org/10.1080/10408398.2016.1225278

Kafashan, A., Joze-Majidi, H., Kazemi-Pasarvi, S., Babaei, A., & Mahdi Jafari, S. (2023). Nanocomposites of soluble soybean polysaccharides with grape skin anthocyanins and graphene oxide as an efficient halochromic smart packaging. *Sustainable Materials and Technologies, 38*, e00755. https://doi.org/10.1016/j.susmat.2023.e00755

Kahyaoglu, L. N. (2024). Intelligent packaging system: A promising approach to reduce food waste. *Current Food Science and Technology Reports, 2*(4), 411–419. https://doi.org/10.1007/s43555-024-00044-6

Khan, A., Ezati, P., & Rhim, J. W. (2024). pH indicator integrated with carbon quantum dots of glucose to monitor the quality of fish and shrimp. *Food and Bioprocess Technology, 17*(2), 554–569. https://doi.org/10.1007/s11947-023-03154-6

Kiaitsi, E., Zanardi, S., Sulyok, M., Medina, A., Ingram, B., Suman, M., & Garcia-Cela, E. (2025). Real-time CO_2 monitoring for early detection of grain spoilage and mycotoxin contamination. *Journal of the Science of Food and Agriculture*. https://doi.org/10.1002/jsfa.70151

Kocatepe, D., Turan, H., Altan, C. O., Keskin, I., & Ceylan, A. (2016). Effect of modified atmosphere packaging on the shelf life of rainbow trout (*Oncorhynchus mykiss*, Walbaum 1792) mince. *Food Science and Technology International, 22*(4), 343–352. https://doi.org/10.1177/1082013215601771

Koshy, R. R., Koshy, J. T., Mary, S. K., Sadanandan, S., Jisha, S., & Pothan, L. A. (2021). Preparation of pH sensitive film based on starch/carbon nano dots incorporating anthocyanin for monitoring spoilage of pork. *Food Control, 126*, Article 108039. https://doi.org/10.1016/j.foodcont.2021.108039

Kostaki, M., Giatrakou, V., Savvaidis, I. N., & Kontominas, M. G. (2009). Combined effect of MAP and thyme essential oil on the microbiological, chemical and sensory attributes of organically aquacultured sea bass (*Dicentrarchus labrax*) fillets. *Food Microbiology, 26*(5), 475–482. https://doi.org/10.1016/j.fm.2009.02.008

Kuswandi, B., & Nurfawaidi, A. (2017). On-package dual sensors label based on pH indicators for real-time monitoring of beef freshness. *Food Control, 82*, 91–100. https://doi.org/10.1016/j.foodcont.2017.06.028

Lako, J., Trenerry, V. C., Wahlqvist, M., Wattanapenpaiboon, N., Sotheeswaran, S., & Premier, R. (2007). Phytochemical flavonols, carotenoids and the antioxidant properties of a wide selection of Fijian fruit, vegetables and other readily available foods. *Food Chemistry, 101*, 1727–1741. https://doi.org/10.1016/j.foodchem.2006.01.031

Lannelongue, M., Finne, G., Hanna, M. O., Nickelson, R., & Vanderzant, G. (1982). Storage characteristics of brown shrimp (*Penaeus aztecus*) stored in retail packages containing CO2-enriched atmospheres. *Journal of Food Science, 47*(3), 911–913. https://doi.org/10.1111/j.1365-2621.1982.tb12743.x

Liang, T., Sun, G., Cao, L., Li, J., & Wang, L. (2018). Rheological behavior of film-forming solutions and film properties from *Artemisia sphaerocephala* Krasch. gum and purple onion peel extract. *Food Hydrocolloids, 82*, 124–134. https://doi.org/10.1016/j.foodhyd.2018.03.055

Liu, Y., Shi, D., Fan, X., Yin, C., Huang, Z., Meng, J., & Gao, H. (2025). Preparation and characterization of a novel polyvinyl alcohol/pectin film containing bromocresol green-alizarin mixed indicator label for monitoring mushroom freshness. *Food Packaging and Shelf Life, 51*, Article 101578. https://doi.org/10.1016/j.fpsl.2025.101578

Ludorf, W., & Meyer, V. (1973). Fische und fischerzeugnisse. Z. Auflage. *Verlag Paul Parey In Berlin und Hamburg*, pp. 209–210.

Luo, Q., Hossen, A., Sameen, D. E., Ahmed, S., Dai, J., Li, S., Qin, W., & Liu, Y. (2023). Recent advances in the fabrication of pH-sensitive indicators films and their application for food quality evaluation. *Critical Reviews in Food Science and Nutrition, 63*(8), 1102–1118. https://doi.org/10.1080/10408398.2021.1959296

Martin, D., Joly, C., Dupas-Farrugia, C., Adt, I., Oulahal, N., & Degraeve, P. (2023). Volatilome analysis and evolution in the headspace of packed refrigerated fish. *Foods, 12*(14), Article 2657. https://doi.org/10.3390/foods12142657

Moradi, M., Tajik, H., Almasi, H., Forough, M., & Ezati, P. (2019). A novel pH-sensing indicator based on bacterial cellulose nanofibers and black carrot anthocyanins for monitoring fish freshness. *Carbohydrate Polymers, 222*, Article 115030. https://doi.org/10.1016/j.carbpol.2019.115030

Morsy, M. K., Zór, K., Kostesha, N., Alstrøm, T. S., Heiskanen, A., El-Tanahi, H., Sharoba, A., Papkovsky, D., Larsen, J., Khalaf, H., Jakobsen, M. H., & Emnéus, J. (2016). Development and validation of a colorimetric sensor array for fish spoilage monitoring. *Food Control, 60*, 346–352. https://doi.org/10.1016/j.foodcont.2015.07.038

Nouraddini, M., Esmaiili, M., & Mohtarami, F. (2018). Development and characterization of edible films based on eggplant flour and corn starch. *International Journal of Biological Macromolecules, 120*, 1639–1645. https://doi.org/10.1016/j.ijbiomac.2018.09.126

Nowzari, F., Shábanpour, B., & Ojagh, S. M. (2013). Comparison of chitosan–gelatin composite and bilayer coating and film effect on the quality of refrigerated rainbow trout. *Food Chemistry, 141*(3), 1667–1672. https://doi.org/10.1016/j.foodchem2013.03.022

Ojagh, S. M., Rezaei, M., Razavi, S. H., & Hosseini, S. M. H. (2010). Effect of chitosan coatings enriched with cinnamon oil on the quality of refrigerated rainbow trout. *Food Chemistry, 120*(1), 193–198. https://doi.org/10.1016/j.foodchem.2009.10.006

Patel, N., Aledda, M., Tafintseva, V., Kohler, A., Liland, K. H., Lintvedt, T. A., & Zimmermann, B. (2025). Spatial distribution of fatty acid composition in salmon fillets. *Journal of Food Composition and Analysis*. https://doi.org/10.1016/j.jfca.2025.108362

Peleg, M. (2022). Models of the water activity effect on microbial growth rate and initiation. *Applied Microbiology and Biotechnology, 106*(4), 1375–1382. https://doi.org/10.1007/s00253-022-11792-7

Pournis, N., Papavergou, A., Badeka, A., Kontominas, M. G., & Savvaidis, I. N. (2005). Shelf- life extension of refrigerated Mediterranean mullet (*Mullus surmuletus*) using modified atmosphere packaging. *Journal of Food Protection, 68*(10), 2201–2207. https://doi.org/10.4315/0362-028X-68.10.2201

Roy, S., & Rhim, J. W. (2021). Anthocyanin food colorant and its application in pH-responsive color change indicator films. *Critical Reviews in Food Science and Nutrition, 61*(14), 2297–2325. https://doi.org/10.1080/10408398.2020.1776211

Sánchez, C. N., Orvañanos-Guerrero, M. T., Domínguez-Soberanes, J., & Álvarez-Cisneros, Y. M. (2023). Analysis of beef quality according to color changes using computer vision and white-box machine learning techniques. *Heliyon*. https://doi.org/10.1016/j.heliyon.2023.e17976

Sharma, H., Fidan, H., Özogul, F., & Rocha, J. M. (2022). Recent development in the preservation effect of lactic acid bacteria and

essential oils on chicken and seafood products. *Frontiers in Microbiology, 13*, Article 1092248. https://doi.org/10.3389/fmicb.2022.1092248

Sümbüloğlu, K., & Sümbüloğlu, V. (2007). Biyoistatistik. Hatipoğlu Press. Ankara, Turkey.

Taherkhani, E., Moradi, M., Tajik, H., Molaei, R., & Ezati, P. (2020). Preparation of on-package halochromic freshness/spoilage nanocellulose label for the visual shelf life estimation of meat. *International Journal of Biological Macromolecules, 164*, 2632–2640. https://doi.org/10.1016/j.ijbiomac.2020.08.177

Tirtashi, F. E., Moradi, M., Tajik, H., Forough, M., Ezati, P., & Kuswandi, B. (2019). Cellulose/chitosan pH-responsive indicator incorporated with carrot anthocyanins for intelligent food packaging. *International Journal of Biological Macromolecules, 136*, 920–926. https://doi.org/10.1016/j.ijbiomac.2019.06.148

Uçak, İ, & Elsheıkh, W. (2023). Antimicrobial quality assessment of sea-bass fillets treated with pomegranate peel extract during refrigerated storage. *Eurasian Journal of Agricultural Research, 7*(1), 37–43.

Venkatachalam, K., Charoenphun, N., Wangtueai, S., Klangbud, W. K., Kraboun, K., Hanpakdeesakul, S., & Wongsa, J. (2025). A review of essential oils in edible films and coatings for seafood preservation: Functional roles, safety, and regulatory considerations. *Trends in Sciences, 22*(9), Article 10415-10415. https://doi.org/10.48048/tis.2025.10415

Wang, A., Tang, F., Chu, Q., Qu, Y., Luo, W., Wang, C., & Xiao, H. (2025b). A ratiometric fluorescent probe for biogenic amine detection and its versatile application in food freshness monitoring, fluorescent ink and biological imaging. *Microchemical Journal*. https://doi.org/10.1016/j.microc.2025.114696

Wang, J., Xie, J., & Mei, J. (2025a). Research progress regarding psychrotrophic pseudomonas in aquatic products: Psychrophilic characteristics, spoilage mechanisms, detection methods, and control strategies. *Foods, 14*(3), 363. https://doi.org/10.3390/foods14030363

Wang, X., & Zheng, Z. (2025). Mechanistic insights into fish spoilage and integrated preservation technologies. *Applied Sciences, 15*(14), Article 7639. https://doi.org/10.3390/app15147639

Wells, N., Yusufu, D., & Mills, A. (2019). Colourimetric plastic film indicator for the detection of the volatile basic nitrogen compounds associated with fish spoilage. *Talanta, 194*, 830–836. https://doi.org/10.1016/j.talanta.2018.11.020

Wu, H., Bak, K. H., Goran, G. V., & Tatiyaborworntham, N. (2024). Inhibitory mechanisms of polyphenols on heme protein-mediated lipid oxidation in muscle food: New insights and advances. *Critical Reviews in Food Science and Nutrition, 64*(15), 4921–4939. https://doi.org/10.1080/10408398.2022.2146654

Xue, H., Gao, Y., Wu, L., Cai, X., Liao, J., & Tan, J. (2025). Research progress in extraction, purification, structure of fruit and vegetable polysaccharides and their interaction with anthocyanins/starch. *Critical Reviews in Food Science and Nutrition, 65*(7), 1235–1260. https://doi.org/10.1080/10408398.2023.2291187

Yingyuad, B. S., Ruamsin, S., Reekprkhon, D., Douglas, S., Pongamphai, S., & Siripatrawan, U. (2006). Effect of chitosan coating and vacuum packaging on the quality of refrigerated grilled pork. *Packaging Technology and Science, 19*, 149–157. https://doi.org/10.1002/pts.717

York, R. K., & Sereda, L. M. (1994). Sensory assessment of quality in fish and seafoods. In F. Shahidi, & J. R. Botta (Eds.), *Seafoods: chemistry, processing technology and quality* (pp. 232–262). Springer New York, NY. 342p. https://doi.org/10.1007/978-1-4615-2181-5

Yoshida, C. M., Maciel, V. B. V., Mendonça, M. E. D., & Franco, T. T. (2014). Chitosan biobased and intelligent films: Monitoring pH variations. *LWT-Food Science and Technology, 55*(1), 83–89. https://doi.org/10.1016/j.lwt.2013.09.015

Yousefi, H., Su, H. M., Imani, S. M., Alkhaldi, K., Filipe, C. D., & Didar, T. F. (2019). Intelligent food packaging: A review of smart sensing technologies for monitoring food quality. *ACS Sensors, 4*(4), 808–821. https://doi.org/10.1021/acssensors.9b00440

Zamfir, L. G., Răut, I., Constantin, M., Corneli, N. O., Firincă, C., Jecu, M. L., & Gurban, A. M. (2025). Assessment of biogenic amines produced by microorganisms as food spoilage indicators by sensitive detection using portable opto-electrochemical tools based on biosensors. *Food Control, 172*, Article 111161. https://doi.org/10.1016/j.foodcont.2025.111161

Zhang, J., Zou, X., Zhai, X., Huang, X., Jiang, C., & Holmes, M. (2019). Preparation of an intelligent pH film based on biodegradable polymers and roselle anthocyanins for monitoring pork freshness. *Food Chemistry, 272*, 306–312. https://doi.org/10.1016/j.foodchem.2018.08.041